HHS Public Access

Author manuscript

Nat Mater. Author manuscript; available in PMC 2023 August 01.

Published in final edited form as:

Nat Mater. 2022 August ; 21(8): 939–950. doi:10.1038/s41563-022-01293-3.

Mechanical checkpoint regulates monocyte differentiation in fibrotic niches

Kyle H. Vining[1,2,3,12,13,15], **Anna E. Marneth**[4,15], **Kwasi Adu-Berchie**[1,2], **Joshua M. Grolman**[1,2,14], **Christina M. Tringides**[5,6], **Yutong Liu**[1,2], **Waihay J. Wong**[3,7], **Olga Pozdnyakova**[7], **Mariano Severgnini**[8], **Alexander Stafford**[2], **Georg N. Duda**[2,9,10], **F. Stephen Hodi**[3], **Ann Mullally**[3,4], **Kai W. Wucherpfennig**[11,✉], **David J. Mooney**[1,2,✉]

[1]John A. Paulson School of Engineering and Applied Sciences, Harvard University, Cambridge, MA, USA.

[2]Wyss Institute for Biologically Inspired Engineering at Harvard University, Boston, MA, USA.

[3]Department of Medical Oncology, Dana-Farber Cancer Institute, Boston, MA, USA.

[4]Division of Hematology, Brigham and Women's Hospital, Boston, MA, USA.

[5]Harvard Program in Biophysics, Harvard University, Cambridge, MA, USA.

[6]Harvard-MIT Division in Health Sciences and Technology, Massachusetts Institute of Technology, Cambridge, MA, USA.

[7]Department of Pathology, Brigham and Women's Hospital, Harvard Medical School, Boston, MA, USA.

[8]Center for Immuno-Oncology Immune Assessment Laboratory at the Dana-Farber Cancer Institute, Harvard Medical School, Boston, MA, USA.

[9]Julius Wolff Institute for Biomechanics and Musculoskeletal Regeneration at Berlin Institute of Health and Charité – Universitätsmedizin, Berlin, Germany.

✉ **Correspondence and requests for materials** should be addressed to Kai W. Wucherpfennig or David J. Mooney. kai_wucherpfennig@dfci.harvard.edu; mooneyd@seas.harvard.edu.

Author contributions

K.H.V., A.E.M., K.W. and D.J.M conceptualized and designed research. F.S.H. advised K.H.V. K.H.V. and D.J.M wrote the original draft. K.H.V., A.E.M., K.A.-B., C.M.T., J.M.G., W.J.W., O.P., M.S., A.M. and A.S. performed research. K.H.V., A.E.M., K.A.B. and Y.L. analysed and visualized data. W.J.W. provided histology images of patient biopsies. G.N.D. provided data on human bone marrow mechanics. W.J.W., O.P., A.E.M. and A.M. provided expertise on MPN and myelofibrosis, as well as mouse *JAK2*-V617F and wild-type monocytes and femurs. A.E.M. performed mouse experiments. All authors contributed review and/or editing of the manuscript.

Online content

Any methods, additional references, Nature Research reporting summaries, source data, extended data, supplementary information, acknowledgements, peer review information; details of author contributions and competing interests; and statements of data and code availability are available at https://doi.org/10.1038/s41563-022-01293-3.

Reporting summary. Further information on research design is available in the Nature Research Reporting Summary linked to this article.

Extended data is available for this paper at https://doi.org/10.1038/s41563-022-01293-3.

Supplementary information The online version contains supplementary material available at https://doi.org/10.1038/s41563-022-01293-3.

[10]Berlin Institute of Health Center for Regenerative Therapies, Berlin Institute of Health and Charité – Universitätsmedizin, Berlin, Germany.

[11]Department of Cancer Immunology and Virology, Dana-Farber Cancer Institute, Boston, MA, USA.

[12]Present address: Department of Preventative and Restorative Sciences, School of Dental Medicine, University of Pennsylvania, Philadelphia, PA, USA.

[13]Present address: Department of Materials Science and Engineering, School of Engineering and Applied Sciences, University of Pennsylvania, Philadelphia, PA, USA.

[14]Present address: Materials Science and Engineering, The Technion–Israel Institute of Technology, Haifa, Israel.

[15]These authors contributed equally: Kyle H. Vining, Anna E. Marneth.

Abstract

Myelofibrosis is a progressive bone marrow malignancy associated with monocytosis, and is believed to promote the pathological remodelling of the extracellular matrix. Here we show that the mechanical properties of myelofibrosis, namely the liquid-to-solid properties (viscoelasticity) of the bone marrow, contribute to aberrant differentiation of monocytes. Human monocytes cultured in stiff, elastic hydrogels show proinflammatory polarization and differentiation towards dendritic cells, as opposed to those cultured in a viscoelastic matrix. This mechanically induced cell differentiation is blocked by inhibiting a myeloid-specific isoform of phosphoinositide 3-kinase, PI3K-γ. We further show that murine bone marrow with myelofibrosis has a significantly increased stiffness and unveil a positive correlation between myelofibrosis grading and viscoelasticity. Treatment with a PI3K-γ inhibitor in vivo reduced frequencies of monocyte and dendritic cell populations in murine bone marrow with myelofibrosis. Moreover, transcriptional changes driven by viscoelasticity are consistent with transcriptional profiles of myeloid cells in other human fibrotic diseases. These results demonstrate that a fibrotic bone marrow niche can physically promote a proinflammatory microenvironment.

The extracellular matrix (ECM) surrounds and supports cells within tissues and undergoes substantial alterations in mechanical properties in a number of disease settings, perhaps best exemplified in fibrotic diseases[1,2]. Although significant effort has been made to understand the impact of matrix stiffness on the molecular and cellular basis of various human diseases[3–5], the matrix also exhibits time-dependent viscoelastic behaviour[6]. We and others have recently shown that matrix viscoelasticity regulates mesenchymal cell fate and spreading in vitro[7–9]. Although the role of mechanobiology on stem cell biology and development has been appreciated[6,10], the impact of matrix viscoelasticity on the immune system and human diseases remains largely unknown.

Myeloproliferative neoplasms (MPNs) are chronic blood cancers that encompasses several subtypes, including polycythemia vera, essential thrombocythemia and primary myelofibrosis (PMF). MPNs are caused by the acquisition of somatic mutations in haematopoietic stem cells, most commonly in *JAK2*, *CALR* or *MPL*; this results in activated JAK-STAT signalling, clonal proliferation of myeloid haematopoietic cells and

in some cases progressive fibrosis of bone marrow ECM, that is, myelofibrosis (Fig. 1a)[2]. Bone marrow biopsies of patients with advanced PMF[11] showed increased reticulin and collagen I compared with patients with early myelofibrosis (Fig. 1b). Myelofibrosis has been traditionally attributed to dysregulated inflammatory cytokine production by haematopoietic cells, which contribute to pathological activation of fibrogenic programmes, ECM deposition and crosslinking[12,13]. Monocytes are a key cellular driver of myelofibrosis[14–16]; and elevated monocyte blood counts (that is, monocytosis) is an adverse prognostic marker for survival in PMF[13]. Further, CD14+ myeloid cells are the principal cellular source of the constitutively overproduced cytokines in PMF[12]. Abnormal mechanical properties of the ECM can regulate monocytes by as-yet unknown mechanisms[2].

We hypothesize that both matrix stiffness and viscoelasticity can independently control monocyte inflammatory polarization and differentiation, which we examine with an artificial fibrotic ECM. As bone-marrow-resident cells pull and push on their surrounding ECM[6], the resistance over time to these mechanical forces is characterized by the ECM's modulus, or stiffness, and viscoelasticity, or stress-relaxation behaviour (Fig. 1c). Here we determine how these mechanical cues regulate monocyte cell fate in vitro and their association with phenotypes of myelofibrosis in bone marrow biopsies and in a relevant myelofibrosis mouse model. Further, we show how the impact of viscoelasticity on monocytes is associated with transcriptional changes in other human fibrotic diseases.

Artificial ECM tunes viscoelasticity

To determine whether the degree of viscoelasticity controls differentiation of human bone-marrow-derived monocytes, we used a three-dimensional, artificial ECM to model the fibrotic and normal bone-marrow matrix, and independently control matrix properties. The mechanical properties of native bone marrow were first identified from fracture haematomas from patients, and exhibited elastic moduli of 1–10 kPa (ref.[17]) and a half-time of stress relaxation of 400 ± 60 s (Fig. 1d). Artificial ECMs were created from interpenetrating networks of alginate and collagen type I fibres[18] to test whether encapsulated primary human bone-marrow-derived monocytes respond to changes in both stiffness and viscoelasticity, which are both controlled independently in this system (Fig. 1e). The polysaccharide alginate is inert to cells[19], while collagen type I is the most abundant matrix component of the bone marrow osteoblastic niche[2]. The extent of ionic crosslinking of alginate by cooperative binding of divalent cations controlled the stiffness of the gels[6,20], while covalent reinforcement of alginate crosslinks with click-chemistry groups (Fig. 1e, inset) made the hydrogels more elastic without changing the adhesion ligand density or gel nano-structure[18]. In this way, we modelled the effect of fibrotic elasticity in malignant bone haematopoietic disease[21,22]. Shear stress relaxation tests confirmed that the relaxation half-time of covalently reinforced gels (NbTz) was slower than that of purely ionically crosslinked gels (Alg) (Fig. 1f), with the latter exhibiting stress relaxation behaviour similar to that of normal bone marrow (Fig. 1d). In spite of their distinct viscoelasticity, both gel types exhibited matching Young's moduli (Fig. 1g) in the stiffer range for human bone marrow (Supplementary Table 1) and for bovine bone marrow[23]. In line with values of relaxation time and loss angle, the more liquid-like Alg gels are termed

'viscous', and more solid-like NbTz ones 'elastic'. Softer hydrogels (~0.75 kPa elastic modulus) that mimic the lower range for bone marrow were also prepared accordingly[18].

ECM viscoelasticity impacts monocyte fate

Next, the impact of matrix stiffness and its relative viscous or elastic nature on the behaviour of monocytes was examined. Human monocytes (Supplementary Table 2) expressing HLA-DR and CD14 were enriched from bone-marrow mononuclear cells (Fig. 2a). As expected, cells cultured in the presence of granulocyte-macrophage colony-stimulating factor (GM-CSF), interleukin 4 (IL-4) and prostaglandin E2 (PGE2) upregulated the antigen-presenting cell markers CD11b, HLA-DR, CD141 and CD11c (Supplementary Fig. 1). Monocytes encapsulated in elastic, stiff gels for 3 d secreted higher levels of matrix metallopeptidase 12 (MMP12) and proinflammatory cytokines and chemokines (Fig. 2b) that contribute to bone marrow fibrosis, including IL-6, CCL2, CCL4 and IL-8 (refs.[12,24]). Cells in viscous gels upregulated galectin 3 and insulin-like growth factor binding protein 7 (IGFBP7), consistent with a less-inflamed and immature phenotype.

Gene expression of cells cultured in elastic, stiff gels clustered separately from all other groups with hierarchical clustering (Fig. 2c) and gene set analysis (Fig. 2c) by a nanoString myeloid panel (Supplementary Data 1). Compared with viscous, stiff gels (Fig. 2c, blue right column), gene sets upregulated by cells in elastic, stiff gels were associated with co-stimulatory molecules, cytokine receptor signalling, non-canonical NF-κB pathway, immunoregulation of lymphoid cells, major histocompatibility complex (MHC) class II antigen presentation and regulation of ECM (Fig. 2d, red text). Principal-component analysis revealed that while major changes were associated with the donor (component 1), as expected, component 2 clearly distinguished the more elastic, stiff hydrogels from the other three matrix conditions (Fig. 2e). Comparison of the viscous, stiff versus elastic, stiff gels revealed that matrix metalloproteases (*MMP12* and *MMP9*) and antigen-presenting cell markers *IDO1* and *RELB* were significantly upregulated in the elastic gels; conversely, in the viscous gels, immature markers were upregulated, including cathepsin G (*CTSG*), neutrophil elastinase (*ELANE*), the *S100A8* subunit of calprotectin, and *IGFBP7* (Fig. 2f). Differential gene expression results across all four mechanical conditions were consistent across two donors (Extended Data Fig. 1), and with a third donor comparing stiff, elastic versus viscous matrix.

Within a cohort of PMF patients, advanced PMF was associated with upregulation of proinflammatory genes *IL8*, *RELB* and *CCL2* (Fig. 2g, red) of a subset of inflammatory markers tested. Conversely, the immature myeloid marker *ARG1* was upregulated in early PMF (Fig. 2g, blue) and expressed by monocytes cultured in viscous gels (Fig. 2f). These results mirrored the effects of viscoelasticity on donor monocytes. Normalized gene expression in advanced PMF (grade 3) was strongly positively correlated ($P < 0.0001$) with normalized gene expression of monocytes in elastic gels (Fig. 2h).

Together, these data show that elastic, stiff ECM directed differentiation of monocytes into dendritic cells, while in contrast, cells in more viscous gels, regardless of stiffness, remained immature monocytes. Cells in elastic, soft gels were less differentiated than those

in the elastic, stiff gels, suggesting that both stiffness and elasticity stimulate monocyte differentiation. Further, gene expression and cytokines expressed by donor monocytes in elastic ECM were consistent with the inflammatory cytokines and signalling pathways of myeloid cells in myelofibrosis patients.

Stiff elastic matrix drives dendritic cell differentiation

High-dimensional analysis of flow cytometry data showed that clusters of individual cells exposed to stiff, elastic and stiff, viscous gels shifted compared to fresh cells (day 0; Fig. 3a, left), and that matrix viscoelasticity generated distinct populations of CD11b+ HLA-DR+ cells (Fig. 3a, right). *K*-means clustering showed that cells in viscous gels predominantly expressed CCR2, CD11b, CD14 and were HLA-DR-low (cluster 1), and cells in elastic gels expressed increased CD11c, CD1c, HLA-DR, PDL1, CD80 and CD141 (cluster 2) (Fig. 3b). Consistent with these findings, the geometric mean fluorescence intensity of HLA-DR was significantly higher in CD11b+ HLA-DR+ cells in elastic gels (Fig. 3c), whereas cells in viscous gels upregulated expression of CCR2, compared with elastic gels (Fig. 3e). The fraction of dendritic cells was significantly upregulated in elastic gels, as indicated by double-positive CD11c+ CD1c+ cells (Fig. 3d) and by CD80+ cells (Fig. 3E). The majority of these cells (~70%) expressed the inhibitory marker PD-L1 in elastic gels and soluble PD-L1 was upregulated in viscous gels (Fig. 2b), which could indicate that dendritic cells generated in an elastic environment inhibit T-cell activation. These flow cytometry results were consistent across three donors (Extended Data Fig. 2). Monocytes in hydrogels were predominantly negative for macrophage marker CD68 (<5%), and neutrophil markers CD15 and CD66b (Supplementary Fig. 2). A fraction of CD11c+ CD163+ DCs were generated in both groups (Fig. 3f), but neither CD11c-CD163+ nor CD68+ macrophages were significantly present.

ECM viscoelasticity and stiffness may impact other cell types involved in myelofibrosis. Monocyte-derived CD14+ CD16+ SLAMF7-high fibrocytes were associated with myelofibrosis in *JAK2*-V617F+ patients[25]. Consistent with these findings, the fraction of cells expressing SLAMF7 (CD319) significantly increased in elastic gels (Fig. 3f). Interestingly, similar effects of elastic matrix on monocyte differentiation were observed in a macroporous system (Supplementary Fig. 3). Increasing the range of stiffness of macroporous elastic ($G' \approx 15$ kPa) and viscous nanoporous ($G' \approx 10$ kPa) hydrogels showed consistent trends as previous results (Supplementary Figs. 3 and 4). Together, these data suggest that stiff, elastic ECM niches are capable of driving dendritic cell differentiation and proinflammatory polarization.

Stiff viscous matrix maintains immature monocytes

Cells in stiff, viscous ECM resisted differentiation into CD1c+ CD11c+ dendritic cells and remained immature CD11b+ cells, as indicated by an increased fraction of CD11b+ HLA-DR-negative/low cells (Supplementary Fig. 2). Bulk RNA-seq analysis of differentially expressed genes in monocytes retrieved from viscous gels showed GATA3, STAT3 and RELA as top-ranked upstream transcription factors (Extended Data Fig. 3a,b). We hypothesized that STAT3 may serve as a marker of immature monocytes in the viscous gels

because STAT3 has been shown to impair dendritic cell differentiation[26]. Imaging in viscous and elastic gels confirmed that phosphorylated STAT3 (pSTAT3, Tyr705) was expressed by cells in viscous gels, while pSTAT3+ cells were significantly reduced in elastic gels (Fig. 3g). STAT3 inhibition with C188–9 was not sufficient to upregulate the fraction of CD1c+ CD11c+ dendritic cells in viscous gels, but did further upregulate dendritic cell differentiation in elastic gels (Fig. 3h). Mechanical regulation of differentiation appeared to be independent of the IL-6–STAT3 axis, as blockade of IL6R did not significantly alter dendritic cell markers in viscous or elastic conditions (Extended Data Fig. 3c). Treatment with interferon-γ (IFN-γ) upregulated IL-6 in elastic matrix (Supplementary Fig. 5). Further evidence that cells in viscous gels are predominantly immature monocytes was shown by the expression of IκB-ζ (gene name *NFKBIZ*, Extended Data Fig. 3D), which is an endogenous inhibitor of non-canonical NF-κB signalling. NF-κB signalling drives dendritic cell differentiation through p100/p50 and RelB (ref.[27]). Staining for IκB-ζ confirmed its expression by immature monocytes in viscous gels (Fig. 3i), which was consistent with high NFKBIZ expression in monocytes in peripheral blood (Fig. 3j). These results were consistent with previous reports of pSTAT3 as a marker of CD14+ HLA-DR-negative/low immature myeloid cells in head and neck cancer[28] and melanoma[29]; and pSTAT3 was shown to down-regulate MHC II expression on blood macrophages[30]. Bone-marrow monocytes in viscous gels may be similar to immature myeloid cells previously identified in these solid tumours. Additional studies are required to determine regulation of STAT3 and NFKBIZ expression in viscous ECM.

Cortical F-actin and Pi3K-γ transduce viscoelasticity

Next, we examined the role of the cytoskeleton on monocyte differentiation in viscous and elastic gels. The cytoskeleton of myeloid cells consists of a cortex of filamentous actin (F-actin) that generates forces by F-actin polymerization (pushing) or actomyosin contractility (pulling). The F-actin cytoskeleton is a key mechanotransducer in development and regeneration[31], is involved in dendritic cell maturation[32] and directs polarization of myelomonocytic cells[33]. Significant upregulation of cortical F-actin was observed in cells in elastic, stiff gels compared with viscous, stiff gels (Fig. 4a). Upregulation of the cortical F-actin cytoskeleton in elastic gels is consistent with differentiation towards dendritic cells, which upregulate F-actin after activation and during homing to the lymph nodes[32,34]. To gain more insight into regulation of F-actin in these cells, we first tested the effects of well-known inhibitors and cytokines related to mechanotransduction and monocyte polarization (Supplementary Table 3 and Supplementary Fig. 6). As expected, inhibition of ROCK with Y27632, Arp2/3 with CK-869, and F-actin with Latruculin-B reduced F-actin assembly in elastic, stiff gels (Fig. 4b). Staining for pan-actin confirmed that non-filamentous actin is expressed by cells in viscous gels, even though cortical F-actin assembly is absent (Extended Data Fig. 4a). Conversely, upregulation of F-actin in elastic gels was impacted by neither the absence of collagen adhesive ligands nor inhibition of actomyosin contractility with blebbistatin (Extended Data Fig. 4b,c), which suggests these effects of elastic gels are independent of contractile cell mechanics or interaction with ECM ligand receptors, and instead relate to cell-pushing forces.

Next, we examined the role of the myeloid isoform of PI3K (PI3K-γ), since it upregulates cortical F-actin assembly and engagement of anchoring to integrin receptors[35]. PI3K-γ regulates the cytoskeleton through Rac1 (ref.[36]), and responds to extracellular hydrodynamic shear stress[37]. PI3K-γ plays an important role in actin polymerization, which drives directional migration in neutrophils[38]. The small molecule inhibitor IPI-549 specifically inhibits this γ isoform of PI3K and is being investigated in clinical trials (Supplementary Table 4)[39]. Further, the rationale for targeting PI3K in MPNs is well established[40,41]. Inhibition of PI3K-γ with IPI-549 significantly reduced F-actin staining of cells in elastic gels (Fig. 4c), and resulted in upregulation of immature marker pSTAT3 (Fig. 4d). Phosphorylated STAT5 (pSTAT5) upregulation in elastic gels was significantly reduced with treatment with the PI3K-γ inhibitor IPI-549 (Supplementary Fig. 7), which was consistent with the role of PI3K in MPN. Treatment of cells in viscous and elastic gels with IPI-549 had no effects on cell viability or relative cell count (Fig. 4e). IPI-549 significantly reduced HLA-DR surface expression and the fraction of CD11b+ CD11c+ cells to a greater extent than treatment with ROCK inhibitor (Fig. 4f), which resulted in a partial effect. Inhibition of F-actin assembly in elastic gels by IPI-549 is consistent with previous reports that PI3K inhibition prevented an increase in F-actin and Rac1 activation induced by IFN-γ stimulation of human-monocyte-derived macrophages[42]. As the mechanosensitive ion channel TRPV4 has been demonstrated to be upstream from PI3K-γ in mechanosignalling[43], we next treated cells with the TRPV4 inhibitor RN-1734. Treatment with RN-1734 had a similar impact on the fraction of CD11c+ CD1c+ dendritic cells in elastic gels as inhibiting PI3K-γ (Fig. 4g). These results were consistent with previous work showing that TRPV4 is regulated by viscoelasticity in vitro[44] and that TRPV4 mediates inflammation in pulmonary fibrosis[45,46]. However, it is expected that TRPV4 is regulated by a number of physical processes and not solely by viscoelasticity.

Together, these findings suggest that monocytes sense their surrounding ECM by intrinsic forces, and upon engaging the elastic resistance of ECM, PI3K-γ is activated to upregulate the F-actin cortex. Our data revealed that PI3K-γ inhibition could potentially suppress inflammation from myeloid cells in elastic fibrotic tissue.

Impact of elasticity is targetable by inhibiting Pi3K-γ

Patient samples and an animal model of MPN were next studied to explore the relevance of the findings to in vivo disease. First, analysis of longitudinal samples from a MPN patient who was untreated and progressed from moderate to overt fibrosis without treatment demonstrated upregulation of cytokines *IL6*, *CCL2* and *CCL4* with disease progression and increasing myelofibrosis grading (Fig. 5a, red line). Next, we assessed whether these markers were impacted by viscoelasticity in healthy donor monocytes. Cells in elastic, stiff gels had higher expression of IL-8, CCL2, IL-6 and CCL4 compared with cells cultured in viscous, stiff cells (Fig. 5b). Moreover, treatment with the PI3K-γ inhibitor IPI-549 significantly downregulated IL-8, CCL2, IL-6 and CCL4 (Fig. 5b). These data are consistent with the reported prognostic value of upregulated IL-8 in MPN[24,47], and IL-8 expression in monocytes isolated from PMF patients[12]. In contrast, IL-6 and IL-8 were only minimally sensitive to JAK-inhibition with ruxolitinib[12].

Subsequently, bone-marrow-derived monocytes were isolated from control mice (Vav-iCre) and a knock-in murine model of MPN harbouring an endogenous *Jak2*-V617F (ref.[48]) mutation (*Jak2*-V617F-Vav-iCre). Similar to studies with human cells, monocytes were encapsulated in viscous, stiff and elastic, stiff artificial ECM to determine the impact of elasticity. As expected, bulk RNA-seq analysis of *Jak2*-V617F monocytes showed that gene expression in the JAK-STAT pathway was upregulated by ECM mechanics (Supplementary Table 5). Gene set enrichment analysis showed that regulation of the actin cytoskeleton was promoted by elasticity (Extended Data Fig. 5a and Supplementary Tables 5–8). Additionally, the expression levels of JAK-STAT pathway markers *Il6* and *Lif* were upregulated by elasticity in *Jak2*-V617F monocytes (Extended Data Fig. 5b). IL-6 and LIF protein levels were increased in conditioned media from elastic versus viscous gels in both Vav-iCre and Vav-iCre *Jak2*-V617F monocytes, and they were further increased in the supernatant from cells with the Vav-iCre *Jak2*-V617F mutation compared with Vav-iCre cells in elastic gels (Extended Data Fig. 5c). Together, these data show that elasticity of ECM upregulates JAK-STAT signalling in both *Jak2*-V617F and wild-type monocytes.

Next, mechanical changes in myelofibrosis, resulting in overt fibrosis in recipient animals, were examined in a transplantation model of *Jak2*-V617F-transduced cells (Fig. 5c). As expected, mice had increased white blood cell, neutrophil and red blood cell counts, and haematocrit level, 8 weeks post-transplant (Fig. 5d). Femurs and spleens from these mice were harvested 5–7 months after transplant. Mice transplanted with *Jak2*-V617F-expressing cells had splenomegaly (Fig. 5d), and histology showed increased megakaryopoiesis in bone marrow and spleen, disruption of splenic architecture, and fibrosis in both organs. Nanoindentation of the femoral bone of these mice showed significantly higher stiffness, or storage modulus, and trending higher solid-like elastic properties, indicated by decreased tan δ, compared with bone marrow of wild-type and transplant-recipient control mice (Fig. 5e). Solid-like, elastic properties of bone marrow (lower tan δ) were positively correlated with a higher fraction of *Jak2*-V617F+ cells and a higher grade of fibrosis (Fig. 5f and Extended Data Fig. 6a). There was no significant correlation with myelofibrosis grade and stiffness, suggesting that change in viscoelasticity, independent of stiffness, is a key feature of the pathologic development of myelofibrosis. The total CD11b myeloid fraction was similar between mice, yet the fraction of CD11b+ Ly6C+ Ly6G− monocytes was increased in fibrotic bone marrow of *Jak2*-V617F recipient mice compared with non-fibrotic Mx1-Cre *Jak2*-V617F knock-in and Mx1-Cre controls (Fig. 5g and Supplementary Fig. 8). We then examined how the PI3K-γ inhibitor IPI-549 affected myeloid differentiation in the retroviral *Jak2*-V617F model. In myelofibrosis bone marrow from mice orally treated with 15 mg kg^{-1} IPI-549 for 2 weeks, the fractions of CD11b+ Ly6C+ LyG− monocytes and CD11c+ MHC II I-A/I-E+ conventional dendritic cells were significantly lower compared with vehicle-treated controls (Fig. 5h). The percentage of CD11b+ Ly6C+ Ly6G+ granulocytes was higher in myelofibrotic bone marrow of mice treated with IPI-549 versus vehicle controls (Extended Data Fig. 6b). Although granulocytes were not assessed ex vivo, these observations were consistent with the reduction of CD11b+ HLA-DR-negative/low monocytes ex vivo in elastic gels, and with their increase with PI3K-γ inhibition (Supplementary Fig. 2c). These data correlate with the involvement of PI3K-γ signalling in mechanosensing of fibrotic bone marrow.

Elastic-dependent transcription is associated with fibrosis

We next examined whether these findings may relate to myeloid inflammation in human fibrotic diseases broadly. Transcriptional profiles of *CD11b*-expressing myeloid single cells in human patients with idiopathic pulmonary fibrosis (IPF) and liver cirrhosis were used to determine whether gene expression of cells in human fibrotic diseases correlated with myeloid cells cultured in elastic versus viscous ECM. High-dimensional analysis of single-cell RNA-sequencing datasets[49,50] (liver cirrhosis GEO accession GSE136103; IPF GSE122960) revealed that the gene expression signature of monocytes identified in encapsulated elastic, stiff ECM (Fig. 6a,b) was enriched in both IPF and cirrhosis compared with in tissue-matched controls of healthy donors. In IPF tissues, cells in clusters 0 and 3 were associated with elastic ECM (Fig. 6c), and significantly upregulated proteases *CTSB* and *CTSD*, macrophage markers *APOC1*, *APOE* and *CCL18*, immature dendritic cell marker *ACP5* (ref.[51]), and MHC class II subunits, *HLA-DPB1* and *HLA-DPA1*. Similar trends were observed in liver cirrhosis clusters 1 and 5 associated with elastic, stiff ECM (Fig. 6d), in which cells upregulated MHC class II subunits and HLA-DR invariant chain (*CD74*), dendritic cell markers (*CLEC10A* and *FCER1A*), and inflamed macrophage and phagocyte markers (*CD5L*, *CD163* and *MARCO*). Markers associated with immature monocytes, *S100A9* and *S100A8*, were downregulated in these profibrotic cells in both IPF and cirrhosis. Although not causal, these data are consistent with cells in elastic gels in vitro, which upregulated antigen-presenting cell markers. Altogether, these findings present additional correlative evidence that the mechanical regulation by viscoelasticity of ECM is an underlying driver of innate inflammation.

There is an unmet clinical need for new therapeutic strategies for myelofibrosis because existing disease management is primarily palliative[2]. Only allogeneic haematopoietic cell transplantation is curative, although few patients are eligible[2]. Here, an artificial ECM system revealed viscoelasticity as a driver of inflamed myeloid cells ex vivo, and PI3K-γ as a potential target of a mechanical checkpoint in myelofibrosis (Fig. 6e). Analysis of a *Jak2*-V617F mouse model suggested that myelofibrosis results in physical changes of the matrix that drive inflammation of myeloid-lineage cells. Although correlation does not provide causal or formal proof, trends observed in an animal model and clinical samples in myelofibrosis and other fibrotic diseases were consistent with the impact of viscoelasticity on monocyte fate ex vivo. Understanding the role of tissue viscoelasticity in myeloid-lineage commitment and monocyte differentiation could impact treatments for fibrotic and proinflammatory disease more broadly.

Methods

Materials synthesis and preparation.

Low-molecular-weight (M_w) ultra-pure sodium alginate (Provona UP VLVG, NovaMatrix) was used for these studies, with an approximate M_w of 32 kDa, ratio of glucuronic acid to mannuronic acid of ≥1.5, and ≤100 endotoxin units per gram, according to the manufacturer. Click-modified VLVG was obtained by covalent coupling of either (4-(1,2,4,5-tetrazin-3-yl)phenyl)methanamine hydrochloric acid (Tz, KareBay Biochem) or 5-(aminomethyl)bicyclo[2.2.1]hept-2-ene (Nb, norbornene methanamine, TCI America) as

previously described[52]. The following protocol results in a 5% degree of substitution, as previously described[18]. First, VLVG alginate was dissolved at 1% w/v in pH 6.5 buffer (0.1 M MES, 0.3 M NaCl). Second, *N*-hydroxysuccinimide and 1-ethyl-3-(3-dimethylam inopropyl)-carbodiimide hydrochloride were added in 5× molar excess based on the number of carboxylic acid groups in this molecular weight alginate (M_w = 32 kDa). Third, Nb or Tz was added at 1 mmol per gram of alginate, and stirred at room temperature for 16 h. Finally, the product was centrifuged, filtered (0.22 μm), purified via tangential flow filtration utilizing a 1 kDa molecular weight cutoff column (Spectrum Labs) using a decreasing salt gradient from 150 mM to 0 mM NaCl in deionized water, followed by treatment with activated charcoal, sterile filtration (0.22 μm), and freeze drying for long-term storage. All chemicals were purchased from Sigma-Aldrich.

Human bone-marrow-derived monocyte isolation.

Primary human monocytes were isolated from fresh human bone marrow donors less than 35 yr old from Lonza (1M-125) by a density gradient with Lymphoprep and SepMate-15 tubes (StemCell Technologies) and negative isolation (EasySep Human Monocyte Isolation Kit, StemCell Technologies). Prior to hydrogel encapsulation on day 0, monocytes were cultured overnight on ultra-low attachment 100 mm dishes (Corning) at 5×10^5 cells per ml in α minimal essential media with glutamax and no nucleosides (Gibco), supplemented with 10% heat-inactivated fetal bovine serum (catalogue number 10082–147, Gibco), 1% penicillin–streptomycin (Thermo), recombinant human GM-CSF (100 ng ml^{-1}, Peprotech), recombinant human IL-4 (200 ng ml^{-1}, Peprotech) and PGE2 (100 ng ml^{-1}, Sigma). Blocking anti-IL6R antibody was used at 1 μg ml^{-1} (MAB227, R&D). The PI3K-γ inhibitor IPI-549 (catalogue number S8330, Selleckchem) was used at 1 μM from a 10 mM stock in DMSO. A complete list of all pharmacological inhibitors and cytokine treatments is given in Supplementary Table 3. Matching data from a total of 14 donors are shown in Supplementary Table 2.

Stress relaxation measurements of bone marrow of fracture haematoma.

Human bone marrow haematoma was harvested as previously described[17] during surgical stabilization of fractures 6 ± 3 d post-fracture and tissues were mechanically tested within 1 h after surgery. Collection of human fracture haematoma was approved by the institutional review board of the Charité – Universitätsmedizin Berlin (EA2/096/11). All patients gave their written consent. Haematoma samples were compressed at a rate of 1 mm min^{-1} until 15% strain, and then stress relaxation was measured over time.

Encapsulation of monocytes in artificial ECM hydrogels.

Hydrogels of interpenetrating collagen type I and alginate were prepared as previously described[18]. Rat tail telo-collagen type I (8–11 mg ml^{-1}, Corning) was neutralized on ice to 6.5 < pH < 7.0. For 1 ml of collagen, the following were mixed sequentially before adding collagen: 100 μl of 10× Hanks' balanced salt solution (HBSS) (without calcium and magnesium, with phenol red, Sigma-Aldrich), 20 μl of 1 M *N*-2-hydroxyethylpiperazine-*N*-2-ethane sulfonic acid (20 mM final concentration, HEPES, Gibco), and 10 μl of 1 M sodium hydroxide (~1% final concentration, NaOH). Ultra-pure unmodified (Alg) or modified alginates (NbTz) were dissolved in a buffered salt solution (HBSS, 20 mM

HEPES) at 5% w/v. A calcium carbonate ($CaCO_3$) slurry was obtained by ultrasonicating (75% amplitude, 15 s) nanoparticles of precipitated $CaCO_3$ (nano-PCC, Multifex-MM, Specialty Minerals) at 100 mg ml^{-1} in sterile water (Water-For-Injection, WFI, Gibco). Immediately prior to casting the hydrogels, collagen was adjusted to pH 7.5 with 1 M NaOH and mixed with $CaCO_3$ slurry on ice for final concentrations of 4 mg ml^{-1} collagen and 0.10% or 0.30% w/v calcium (soft and stiff, respectively). Cells were retrieved from culture and suspended at 75×10^6 cells per ml in HBSS/HEPES on ice and added to the collagen–calcium solution for a final concentration of 5×10^6 cells per ml. Alginate was stirred with the gel solution on ice for a final concentration of 1.5% w/v total alginate. For click-modified alginates (NbTz), the ratio of Alg-Nb to Alg-Tz was adjusted depending on calcium condition (Supplementary Table 1). Immediately before gelation an appropriate amount (4× molar excess of the calcium concentration) of freshly dissolved glucono-δ-lactone (0.4 g ml^{-1} in HBSS/HEPES, GDL, EMD Millipore) was added during rapid stirring. Overmixing was carefully avoided to minimize shearing of cells. The resulting solution was quickly transferred by micropipettes to a microwell of multi-well MatTek plates. Initial gelation for 1 h was performed at 37 °C in tissue culture incubator, followed by equilibration in 1 ml of HBSS/HEPES buffer at 37 °C for 1 h, and then replacement of buffer with cell culture media. See Supplementary Methods for fabrication of macroporous collagen–alginate scaffolds.

Rheological characterizations of artificial ECMs.

Rheological characterization of the resulting IPN hydrogels was performed on a stress-controlled rheometer (AR-G2, TA Instrument) using a 20 mm cone plate as previously described[18]. Hydrogel solution (75 μl) of was loaded immediately onto the Peltier plate after mixing. A humidity chamber was used to prevent dehydration. Oscillatory rheology was used to measure the storage modulus (G'), loss modulus (G'') and loss angle (δ) after equilibrium was achieved. Rheological tests included an oscillatory time-sweep for 3 h at 25 °C (1 Hz, 1% strain), followed by oscillatory frequency sweep (1% strain, 0.1–10 Hz). A shear stress relaxation test was performed by applying 10% shear strain in 1 s and then maintaining the strain over time while recording shear stress for 2–12 h. The time sweep at 25 °C was used to avoid carbon dioxide and nitrogen gas bubbles, which cause rheological artifacts.

Luminex and ELISA assays on conditioned media.

Conditioned media from each well was collected and stored at −80 °C. For analysis, conditioned media was thawed, centrifuged at 1,000*g* for 5 min, and the supernatant was diluted appropriately in diluent. Measurements of diluted samples were performed according to the manufacturer's instructions for the Luminex (R&D) or ELISA assays (IL-8, Biolegend; IL-6, Biolegend; CCL2, Biolegend; IL-1-RA, R&D; CCL4, Biolegend; LIF, Biolegend). The results are reported in pg or ng per sample by multiplying by total media volume per sample. A heatmap of average cytokine expression with unsupervised hierarchical clustering was generated using the pheatmap package in R[53].

Retrieval of cells from hydrogels.

Hydrogels were digested with 100–150 µl of 300 U ml^{-1} collagenase IV (Worthington) and 34 U ml^{-1} of alginate lyase (Sigma-Aldrich) in DBPS + Ca/Mg, 0.5% BSA at 37 °C for 15 min, followed by addition of another 100–150 µl of 300 U ml^{-1} collagenase IV and incubation at 37 °C for 15 min. Next, 0.5 ml wash buffer (DPBS without Ca/Mg, 2 mM EDTA, 0.5% BSA) was added, and the samples were transferred to a deep-bottom 1.2 ml 96-well plate. The plate was centrifuged at 400*g* for 5 min at 4 °C and the supernatant discarded. A final set of washes was performed with cold 0.2 ml wash buffer on ice, followed by centrifugation at 400*g* for 5 min at 4 °C to obtain a clean cell pellet. Cell counts and viabilities were measured by viability staining and flow cytometry (MUSE) to confirm successful isolation and to quantify cell yields.

nanoString nCounter hybridization of lysed cells and analysis.

Cells (~100,000) from each sample were suspended in 0.05 ml RNA-later (ThermoFisher) at 4 °C until analysis. The RNA-later was diluted with 4-fold volume of cold PBS (without Ca or Mg). Samples were centrifuged at 800*g* for 10 min at 4 °C and lysed and homogenized at 10,000 cells per µl with RLT buffer (Qiagen) + 1% 2-mercaptoethanol (Sigma). A volume of 1.5 µl of lysates were used in the nanoString hybridization reaction and the remainder was stored at −80 °C. nCounter Elements (nanoString) hybridization was performed according to the manufacturer's instructions. A list of panel targets is given in the Supplementary Data. TagSets (nanoString) were thawed and stored on ice. Aliquots of master stocks of probe A and B (IDT) were thawed and diluted to 0.6 nM and 3 nM working pools, respectively. Hybridization buffer (nanoSTring) was mixed sequentially with Probe A and B working pools, followed by the addition of 1.5 µl of RNA lysate. The total reaction volume was adjusted with RNA-ase-free water to 15 µl. Subsequently, hybridization was performed for 20 h at 67 °C on a thermocycler, followed by ramping to 4 °C. Hybridized samples were loaded on nanoString cartridges for analysis. Data were analysed using nSolver and nCounter Advanced Analysis.

Immunostaining and flow cytometry analysis.

Cells isolated from hydrogels were stained with dead cell stain (Thermo) before blocking with FcRx and staining with mouse antibodies for anti-human PDL1 (BV421), CD14 (BV510), CD45RA (BV570), CD11c (BV711), CD11b (GFP or PE-Dazzle-594), CD1c (PE), CD141 (PE-Dazzle-594), CD80 (PE-Cy7), SLAM-F7 (PE-Cy7) and HLA-DR (APC Fire 750). Brilliant Violet staining buffer (BD Biosciences) was used during staining. All flow antibodies were obtained from Biolegend. Flow analysis was performed on Fortessa LSRII with anti-mouse compensation beads (BD Biosciences). Gating was performed on Cells-Single Cells-Live Cells-CD11b+ HLA-DR+ with fluorescence-minus-one controls. Log-scale flow cytometry data were analysed with R v.3.6.2. Gating for each marker was defined as the mean of fluorescence-minus-one control (FMO) fluorescence intensity + 3 × s.d. of FMO fluorescence intensity, assuming FMO fluorescence followed a normal distribution. For dimension reduction for day 0, viscous, and elastic conditions, 15,000 live cells were selected for each condition, and Non-linear dimensionality reduction was performed by t-distributed stochastic neighbor embedding (tSNE) with the package Rtsne

v.0.15. For dimension reduction for viscous and elastic conditions, 15,000 CD11b+ HLA-DR+ double-positive cells were selected for viscous and elastic conditions for tSNE calculation, and cells were clustered into two populations with *k*-means clustering.

Whole-mount immunohistochemistry and multiphoton confocal imaging.

Hydrogels containing cells were initially cast in microwells of MatTek plates or dishes. They were prepared for whole-mount immunohistochemistry by aspiration of cell culture media and fixation overnight at 4 °C in 4% paraformaldehyde in HBSS buffer with 20 mM HEPES and 2.5 mM $CaCl_2$. Gels were washed three times in PBS, followed by blocking and permeabilization overnight at 4 °C in PBS with 10% goat serum (Jackson Labs), 1% BSA (Sigma) and 1% Triton X-100 (Invitrogen). Primary antibody labelling was performed overnight at 4 °C in staining buffer of PBS with 6% BSA and 0.1% Triton X-100. Primary antibodies used for these studies included rabbit anti-pSTAT3 (1:100, Tyr705, Cell Signaling, #9145), rabbit anti-NFKBIZ (1:100, Cell Signaling, #9244) and rabbit anti-pan-Actin (1:100, Cell Signaling, #8456). Gels stained with primary antibodies were washed twice with staining buffer for 30 min each at room temperature on a shaker, followed by overnight at 4 °C on a shaker. Secondary antibody and F-actin staining was performed overnight at 4 °C in staining buffer. The secondary antibody used for these studies was goat anti-rabbit Alexa Fluor-633 (1:100, H&L, heavily cross-adsorbed, ThermoFisher). Phalloidin-546 (1:1,000, ThermoFisher) was used to stain F-actin. Next, samples were washed twice with staining buffer for 30 min each at room temperature on a shaker, followed by overnight at 4 °C on a shaker. Samples were mounted in Prolong Gold + DAPI (ThermoFisher) and stored at 4 °C before imaging. Samples were imaged with Leica confocal and multiphoton laser excitation (820 nm) with non-descanned detector settings of 430–480 nm for DAPI, 565–605 nm for anti-546 and 625–675 for anti-633. *Z*-stacks were obtained of 2.5-μm-thick sections from 25 to 175 μm. Quantifications of mean fluorescence intensity (MFI) are from background-subtracted maximum-intensity projections of individual cells.

Jak2-V617F knock-in mouse model and bone marrow monocyte isolation and hydrogel encapsulation.

Femurs and tibia from 25- to 30-week-old male or female Vav-iCre or Vav-iCre *Jak2*$^{V617F/+}$ mice[54] were crushed, cells were filtered and red blood cells were lysed using BD erylysis buffer. Monocytes were isolated using a negative selection isolation kit (Stem Cell Technologies) and cultured on ultra-low-attachment tissue culture plates (Corning) overnight with recombinant mouse animal-free GM-CSF (100 ng ml^{-1}, PeproTech), recombinant mouse animal-free IL-4 (200 ng ml^{-1}, PeproTech) and 100 ng ml^{-1} PGE2 (Sigma), similar to the cultures with human cells. After overnight culture, monocytes were encapsulated in hydrogels (day 0) and cultured with the cytokines for 3 d. Then, cells were retrieved from the hydrogels as described above and lysed for RNA isolation (Purelink RNA Microscale Kit, Thermo). RNA was quantified and quality checks were performed by TapeStation, nanoDrop, and RiboGreen. cDNA libraries were prepared for RNA sequencing by Kapa mRNA Hyperprep and normalized by quantitative polymerase chain reaction.

Retroviral *Jak2*-V617F bone marrow transplant model and IPI-549 treatments.

Haematopoietic cells from male donor mice were harvested by crushing femurs, tibia, humeri and spine followed by a 100 μm filtration step. Red blood cells were lysed using BD Pharm Lyse (BD), after which cells were filtered using 70 and 40 μm cell strainers. Cells were incubated with c-kit/CD117 magnetic microbeads (Miltenyi Biotec), washed, and c-kit+ haematopoietic stem- and progenitor cells were positively selected using an autoMACS (Miltenyi Biotec). C-kit+ cells were cultured at 1 million cells per ml in serum-free expansion medium (StemCell Technologies) supplemented with 50 ng ml^{-1} rmSCF (Preprotech), 50 ng ml^{-1} rmTPO (Preprotech) and 1% penicillin–streptomycin (ThermoFisher Scientific). One day after isolation, pMEGIX *Jak2*-V617F or pMEGIX empty vector retrovirus was spun onto retronectin (Takara)-coated plates (2800 r.p.m., 90 min, 37°C) and viral supernatant was largely aspirated. C-kit+ cells were added (in serum-free expansion medium with 50 ng ml^{-1} rmSCF, 50 ng ml^{-1} rmTPO, 1% penicillin–streptomycin and 4 μg ml^{-1} polybrene (Fisher Scientific)), and the plate was spun down for another 10 min at 1500 r.p.m. One day after transduction, cells were harvested, washed and resuspended in PBS. Female recipient mice (Taconic Biosciences) were lethally irradiated with two doses of 500 cGy irradiation, 6 h apart. Six hours after the first irradiation, recipient mice were retro-orbitally injected with 200,000–500,000 donor cells. Peripheral blood was drawn retro-orbitally into EDTA-coated tubes and subjected to complete blood counts on an Advia 2120i (Siemens) or an XN-N series multispecies haematology analyser (XN-1000V; Sysmex). Mice were analysed 5–7 months after transplant. One femur per mouse was harvested to measure bone marrow mechanics. Remaining femur and spleen were fixated in 10% formalin, paraffin-embedded, sectioned and subjected to haematoxylin–eosin and reticulin staining. Reticulin stains were blindly scored for myelofibrosis by an experienced pathologist.

For vehicle and IPI-549 treatments, mice were randomly assigned into treatment groups with similar peripheral blood GFP% at 19 weeks post-transplant. IPI-549 or vehicle (10% DMSO (Sigma-Aldrich), 5% 1-methyl-2-pyrollidone (NMP, Sigma-Aldrich), 85% polyethylene glycol 400 (PEG400, Sigma-Aldrich)) were administered daily p.o. for 2 weeks starting 20 weeks post-transplant. Bone marrow was harvested 2 weeks later and subjected to flow cytometry staining. Antibodies were from BD Biosciencies (CD45.2-V500) and Biolegend (CD11b-Pacific Blue, Ly6C-APC, Ly6G-BV605, Ly6G-PerCP/Cy5.5, CD11c-APC-Fire750, MHC class II I-A/I-E-PE-Cy7). Flow cytometry data were analysed on a Cytek Aurora (Cytek Biosciences) and analysed using FlowJo. Mice with <2% GFP+ cells within the CD45.2+ bone marrow fraction did not develop myelofibrosis and were excluded from the analyses.

Jak2-V617F knock-in transplant model.

Bone marrow cells from two uninduced age- and sex-matched C57BL/6 donors (Mx1-Cre and Mx1-Cre *Jak2*-V617F (ref.[54]) were harvested and c-kit+ cells were isolated as described above. c-kit+ cells (180,000) were retro-orbitally injected into lethally irradiated (2 × 5Gy, 6 h apart) 8- to 11-week-old female recipients (Taconic Biosciences). Four weeks post-transplant, mice were injected i.p. three times with 8 μg g^{-1} poly(I:C) (Cytiva). Mice were killed and analysed 7 months later as described above.

Nanoindentation of mouse femur bone marrow mechanics.

Femurs from 5- to 7-month-old mice were freshly dissected, snap-frozen with liquid nitrogen vapour, freeze-fractured with a cryotome blade into 0.5-mm-thick axial cross sections, and stored at 4 °C in PBS overnight. Mechanical testing was performed using an Agilent G200 nanoindenter (Agilent) with a 90° diamond conical probe tip with a 50 μm radius (DCMII, Micro Star Technologies) to enable measurement of bulk properties[55]. The tip area function was calibrated using fused quartz, and a punch diameter of 45.153 μm was calculated at a 5 μm precompression depth. Tip-to-optics calibrations were done before each experiment with thin film of melted wax. A 3 × 3 array of indents with 200 μm spacing was generated, with tip-cleaning indents performed subsequent to each measurement. Tests were run in continuous stiffness measurement mode to afford the complex shear modulus under the shear mode[56] at room temperature at a constant frequency of 110 Hz. Storage modulus G' was measured as the energy stored during one oscillation cycle, and loss modulus G'' was measured as the energy dissipated during an oscillation cycle[57]. Poisson's ratio (ν) was estimated for the two different-sized rounded conical probes used and was found to be approximately 0.45, corresponding to values confirmed in the literature for bulk measurements of hydrogel polymers and tissues[58].

Bulk RNA-seq analysis of mouse monocytes.

Sequenced mRNA from *Jak2*-V617F Vav-iCre and wild-type *Jak2*-Vav-iCre mice were aligned and quantified using salmon[59], and were mapped unto an Ensembl GRCm38 reference transcriptome index. Transcripts were then converted to gene IDs using the AnnotationDbi[60], RMaria[61] and tximport[62] packages in R. Differentially expressed genes, defined as genes with an adjusted P value ≤0.1, were then determined using DEseq2 (ref.[63]). Pathway analysis was performed on log-transformed gene counts using the GAGE package in R[64]. Heatmaps of expression levels of genes that correspond to pathways of interest (for example, JAK-STAT) were then plotted using pheatmap with hierarchical clustering in R[53].

Human study population and gene expression analysis.

The pathology archives at Brigham & Women's Hospital (BWH) and Massachusetts General Hospital (MGH) were queried to identify patients with myelofibrosis on bone marrow biopsy obtained between 2005 and 2016, as previously described[11]. Patients diagnosed with myelodysplastic syndrome/MPN overlap disease and those who had progressed to acute leukaemia, received treatment with chemotherapeutic agents for prior cancer diagnoses, or had undergone stem cell transplantation were excluded. BWH specimens were fixed in Bouin's fixative and decalcified in RapidCal Immuno (BBC Biochemical) for 15 min, followed by routine processing. Specimens from MGH were fixed in B-plus fixative for a minimum of 4 h and decalcified in RapidCal Immuno for 30 min, followed by routine processing. Histologic review and fibrosis grading were performed by W.W., R.P.H. and O.P. based on consensus, using the 2016 WHO Revised Classification of Myeloid Neoplasms[65]. RNA was isolated from 50 μm sections prepared from fixed, decalcified and paraffin-embedded bone marrow biopsies using a Qiagen RNeasy Kit, as previously described[11]. Multiplexed mRNA quantification was performed using a Nanostring nCounter GX Human Inflammation V2 Kit and analysed by nSolver and nCounter Advanced Analysis. The study

was conducted in accordance with the principles set forth by the Declaration of Helsinki and the requirement for informed consent was waived by the institutional review board.

Analysis of single-cell RNA-seq datasets.

Single cell RNA-seq count matrices from GEOs GSE122960 (IPF dataset) and GSE136103 (liver cirrhosis dataset) were imported into R using the Seurat package and filtered for (1) 200 minimum features per cell, (2) 10 minimum cells per feature, (3) mitochondrial gene percentage ≥15% and (4) myeloid cells expressing ITGAM. Filtered cells from healthy and diseased patients from each dataset were SCTransformed and integrated, after which PCA, cluster analysis and UMAP analysis were performed. To determine the relative expression of markers associated with cells from the elastic or viscous ECM, the average expression of genes differentially expressed in elastic or viscous modules from nanoString experiments were calculated for each cell using Seurat's AddModuleScore function[66,67]. The formula: $10^{\text{elastic\_module}}/10^{\text{viscous\_module}}$ was then used to find the corresponding ratio of elastic to viscous module per cell, where elastic_module and viscous_module are the average expression levels of genes differentially expressed in elastic and viscous ECM for each cell, respectively. Statistical tests comparing relative expression levels of the elastic module for cells from healthy and diseased tissues were performed using the Wilcoxon rank sum test with false discovery rate (FDR)-adjusted *P* values. For comparing the ratios of elastic to viscous modules for cells in each cluster, clusters with mean ratios of ~1 were first determined: cluster 2 for IPF and cluster 3 for liver fibrosis. All other clusters were then compared with these clusters pairwise using the Wilcoxon rank sum test with FDR-adjusted *P* values.

Statistical analysis.

Statistical analysis was performed on Prism GraphPad software. Normality tests were performed to determine Gaussian distribution. Statistical tests included one-way analysis of variance (ANOVA) and post-hoc tests for multiple comparisons or Student's *t*-tests for comparison between two groups. Brown–Forsythe and Welch ANOVA or *t*-test with Welch correction were used when variances significantly differed between groups. Non-parametric Mann–Whitney tests were used to compare two groups that did not follow normal distribution. *P* values <0.05 were assumed to be significant in all analyses. Error bars represent s.e.m., unless otherwise noted. Supplementary Table 9 shows the results of statistical tests for all data presented. The statistical test in Fig. 6 is explained above (Analysis of single-cell RNA-seq datasets).

Extended Data

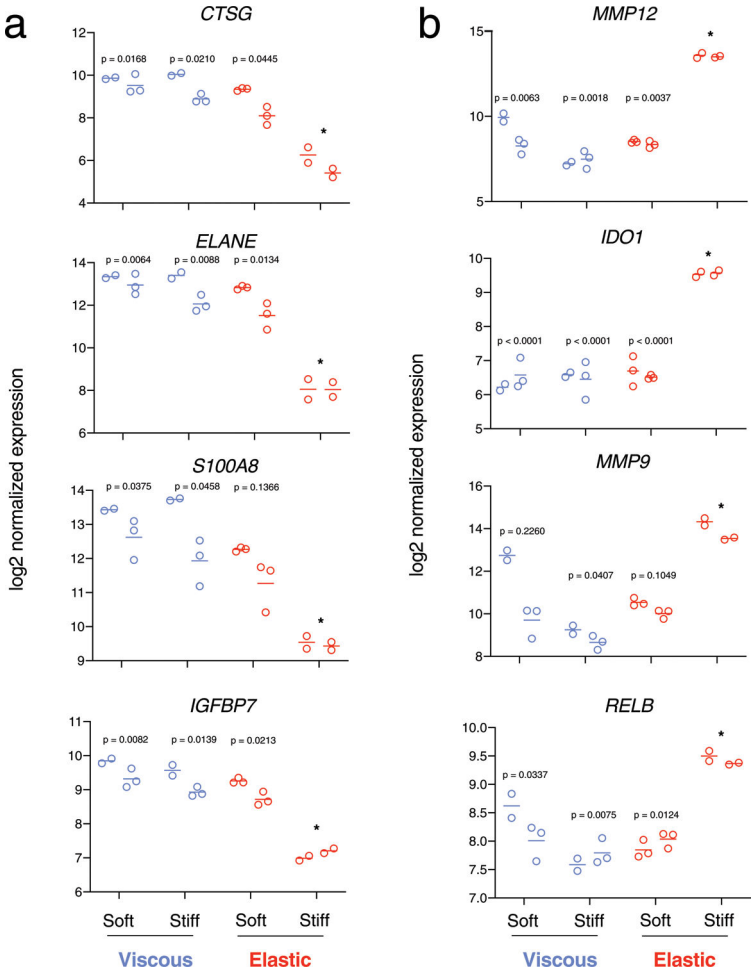

Extended Data Fig. 1 |. Related to Fig. 2. Nested scatterplots of normalized gene expression of markers upregulated in cells in viscous and soft-elastic gels (A) and stiff-elastic gels (B).

Each set of data points represents biological replicates from a particular donor (the two sets of data points at each experimental condition represent cells from the n = 2 donors). Soft ~ 0.75 kPa, Stiff ~ 7.5 kPa elastic moduli. P-values indicate statistical significance ($p < 0.05$) compared to stiff-elastic gels (*, asterix) of nested one-way ANOVA with Tukey's multiple comparisons tests. All analyses were performed at 3 days after encapsulation.

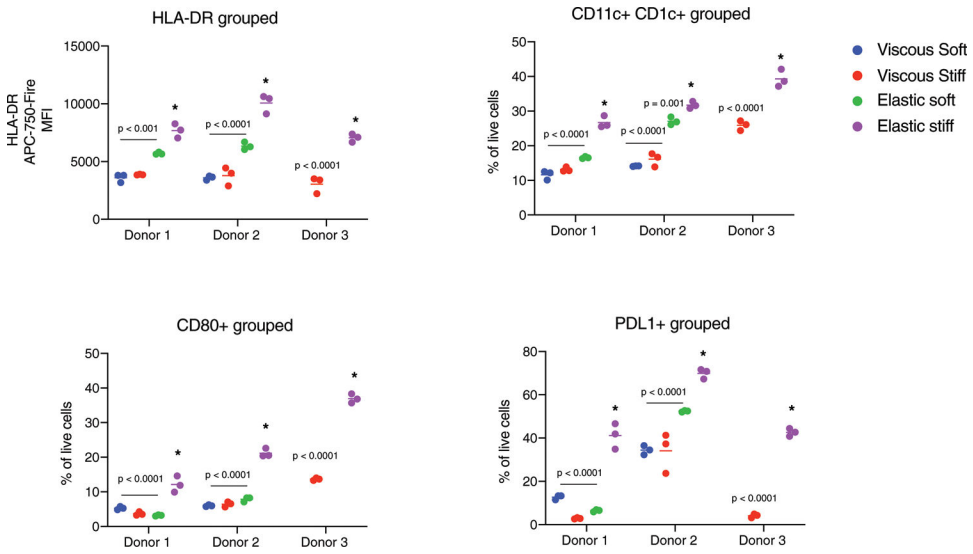

Extended Data Fig. 2 |. Related to Fig. 3. Nested scatterplots of flow cytometry performed on samples from n = 3 donors.

HLA-DR mean fluorescence intensity (MFI), fraction of live cells expressing dendritic cell differentiation markers CD11c + CD1c +, CD80 +, and PDL1 + gated on live-HLA-DR + cells for soft viscous (blue), stiff viscous (red), soft elastic (green), and stiff elastic (purple) gels. P-values indicate statistical significance ($p < 0.05$) of n = 3 biological replicates of two-way ANOVA with Tukey's multiple comparisons tests compared to stiff elastic gel within each donor (asterix). All analyses were performed at 3 days after encapsulation.

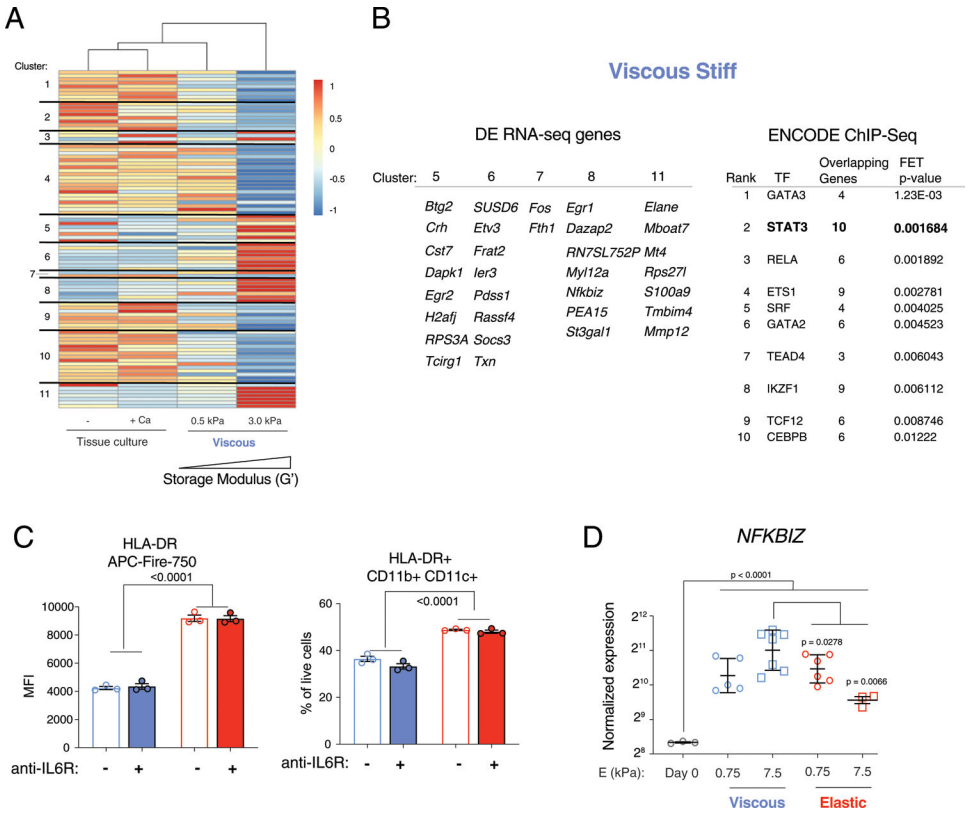

Extended Data Fig. 3 |. Related to Fig. 3. STAT3 transcription factor is associated with differentially expressed genes in stiff viscous hydrogels.

A) Unsupervised hierarchical clustering of differentially expressed genes from bulk RNA sequencing. Cells from soft and stiff viscous gels are compared to cells in non-adherent tissue culture with or without calcium control. The calcium control are cells exposed to free calcium released from an empty hydrogel. Markers were separated into 11 clusters associated with patterns of gene expression. **B)** Clusters 5, 6, 7, 8, and 11 were associated with genes upregulated in stiff viscous conditions. These markers were put into the ENCODE ChIP-Seq database, which identified STAT3 as one of the top ranked transcription factors involved in regulating these genes. **C)** Flow cytometry of HLA-DR MFI and CD11b + CD11c + cells (gated on live-HLA-DR +) with blocking anti-IL6R antibody (1μg/ml), n = 3 biological replicates. **D)** Normalized gene expression of *NFKBIZ* at Day 0 prior to encapsulation and after 3 days in viscous and elastic gels of soft (0.75 kPa) and stiff (7.5 kPa) elastic modulus. Data points indicate biological replicates from n = 2 donors for viscous and elastic gels, and n = 1 donor for day 0 control. P-values<0.05 indicate statistical significance of one-way ANOVA with Tukey multiple comparisons test. Experiments were repeated with at least two donors. Data are presented as mean values + /− SEM.

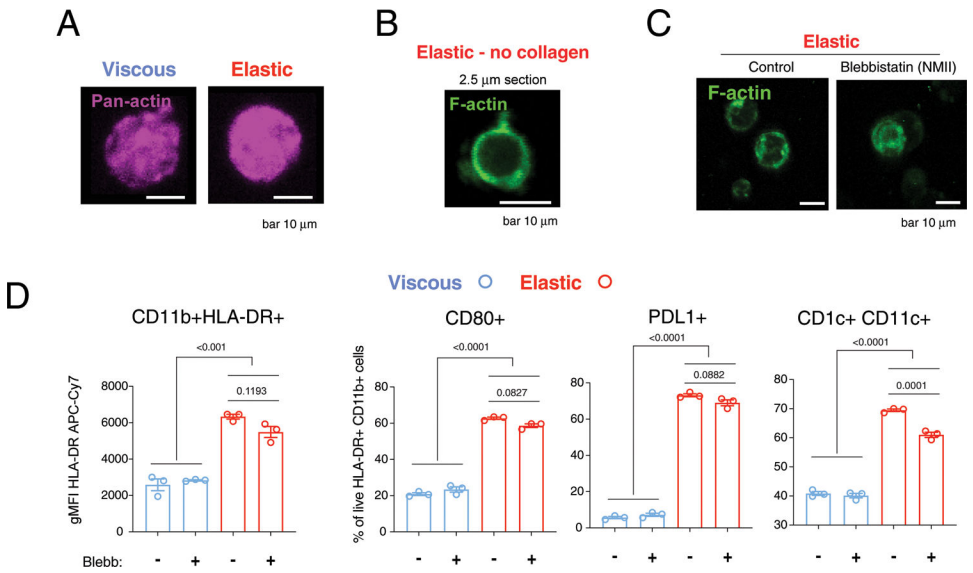

Extended Data Fig. 4 |. Related to Fig. 4. F-actin in elastic gels is independent of collagen adhesive ligands and actomyosin contractility.

A) Pan-actin staining of cells in viscous and elastic gels. **B)** F-actin staining of cells in elastic gels without collagen. **C)** F-actin staining with or without inhibition of actomyosin contractility by non-muscle myosin-II by blebbistatin (10 μM). **D)** Flow cytometry for dendritic cell differentiation markers with or without blebbistatin. Images are maximum intensity projections of representative cells. Scale bar 10 um. Data points indicate n = 3 biological replicates from 1 donor. P-values<0.05 indicate statistically significant difference by ordinary one-way ANOVA with Tukey multiple comparisons test. All analyses were performed at 3 days after encapsulation. Data are presented as mean values + /− SEM.

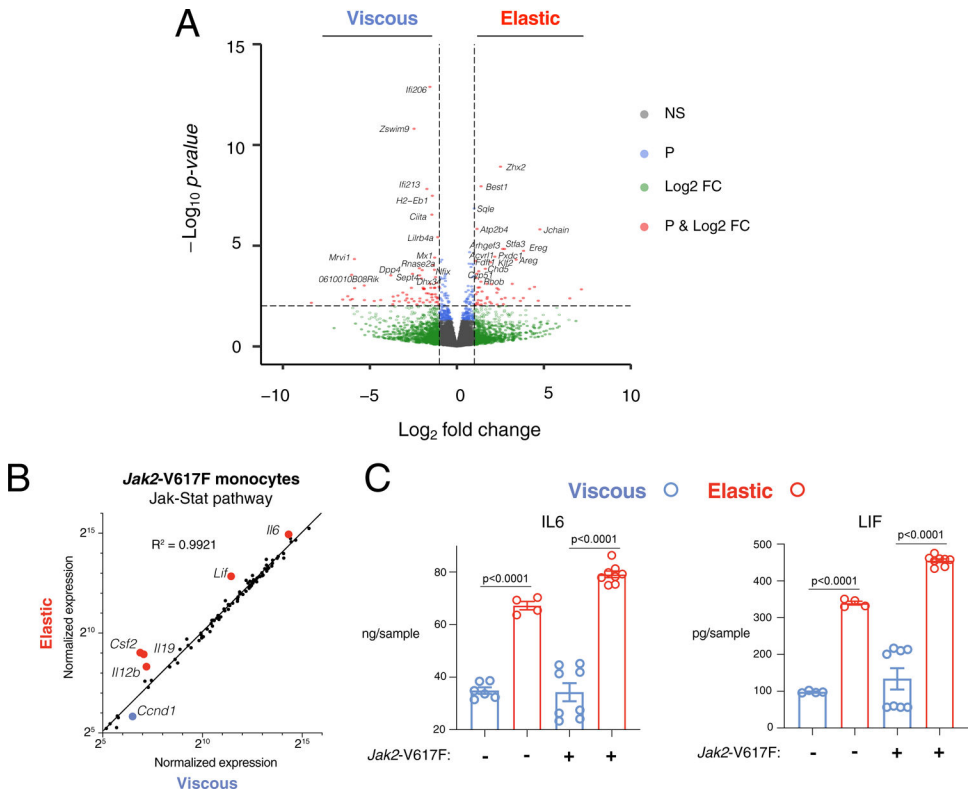

Extended Data Fig. 5 |. Related to Fig. 5. Viscoelasticity impacts *Jak2* signaling in *Jak2*-V167F monocytes.

A) Volcano plot of global transcriptome of differentially expressed genes comparing mouse *Jak2*-V617F monocytes in stiff, elastic versus stiff, viscous gels. Bulk RNA-sequencing was performed in duplicate. Genes marked in red are above thresholds of both fold change = 2^1 and p-value = 10^{-2} threshold (dotted lines). Green indicates genes above fold change threshold, but below the p-value threshold. Blue indicates genes above the p-values threshold, but below the fold change threshold. Grey indicates genes that are not significantly differentially expressed. Data was obtained from n = 2 biological replicates. **B)** Normalized expression of JAK-STAT pathway genes in *Jak2*-V617F monocytes cultured in elastic versus viscous hydrogels, with linear regression fit (black line). Genes enriched in elastic gels are marked in red and appear above the linear regression (viscous in blue). Data points indicate mean normalized expression of n = 2 biological replicates from a single experiment (one of each gender). **C)** IL6 and LIF levels of conditioned media from WT or *Jak2*-V617F monocytes in viscous (blue) or elastic (red) hydrogels. Data shown from a single experiment with n samples as individual data points collected from n = 2 biological replicates (one of each gender). P-value<0.05 indicates statistically significant difference by Brown–Forsythe and Welch ANOVA test with Dunnett's T3 multiple comparisons test.

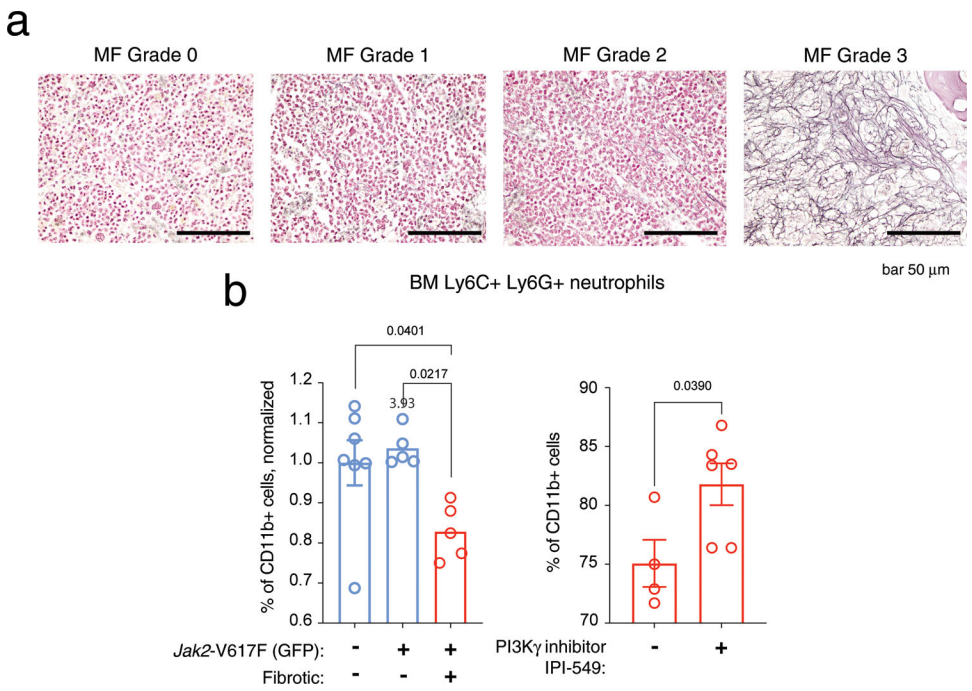

Extended Data Fig. 6 |. Related to Fig. 5. Pathologic grading of model of MF and flow cytometry analysis of BM neutrophils.

A) Representative MF grading of histologic sections from femurs of recipient retroviral *Jak2*-V617F mice, repeated n = 3 independent experiments. 60x objective. **B)** Flow cytometry to determine the fraction of bone marrow Ly6C + LY6G + neutrophils in mouse models of fibrotic (pMEGIX *Jak2*-V617F) and non-fibrotic (Mx1-cre *Jak2*-V617F) MPNs, gated on CD11b + cells. In the left panel, mice were untreated. Values were normalized to empty-vector controls, and data shown is from n = 3 independent cohorts of mice. In the right panel, cells were analysed from fibrotic pMEGIX *Jak2*-V617F recipient mice and treated with either vehicle control (−) or IPI-549 (+) daily for 2 weeks with oral gavage of 15 mg/kg IPI-549 10% DMSO/5%NMP/85% PEG400. Data points indicate n biological replicates from 1 independent experiment. P-values <0.05 indicate statistically significant differences of one-way ANOVA with Tukey multiple comparisons test or unpaired two-tailed Student's t test. Data are presented as mean values + /− SEM.

Supplementary Material

Refer to Web version on PubMed Central for supplementary material.

Acknowledgements

At the Wyss Institute, we thank T. Ferrante for assistance with imaging, and group members D. Zhang and A. Gonzalez-Pujana for their assistance and feedback on this work. At Massachusetts General Hospital, we thank D. Lagares for his feedback and editing. At the Massachusetts Institute of Technology, the authors thank T. Gierahn and the BioMicroCenter for assistance with bulk RNA-sequencing. At Dana-Farber Cancer Research Institute, we thank C. Laurore for technical assistance. Part of this work was performed at the Bauer Core Facility at Harvard University. We thank S. Reinke and his Cell Harvest Unit of the Berlin Institute of Health Center for Regenerative Therapies and the Charité for supply of the human fracture haematoma samples. We acknowledge Sysmex America, M. Sola-Visner and her laboratory members E. Nolton and P. Davenport (Boston Children's Hospital) for kindly sharing Sysmex equipment for complete blood counts. Research reported in this

manuscript was supported by the National Cancer Institute of the National Institutes of Health under award number U01CA214369 (D.J.M.), the National Institute of Dental & Craniofacial Research of the National Institutes of Health under award numbers K08DE025292 and K99DE030084 (K.H.V.), the Federal Drug Administration R01FD006589 (D.J.M.), and the Harvard University Materials Research Science and Engineering Center (grant DMR 1420570). The content is solely the responsibility of the authors and does not necessarily represent the official views of the National Institutes of Health. Parts of the work were supported by the Einstein foundation and the German Research Foundation in the context of the DFG FOR 2165 grant and CRC 1444 grants (G.N.D.). A.E.M. was supported by a long-term fellowship from the European Molecular Biology Organization (EMBO, ALTF 268-2017) and Horizon award from the US Department of Defense (W81XWH-20-1-0904). A.M. is a Scholar of the Leukaemia and Lymphoma Society (LLS). O.P. was supported by a Brigham and Women's Hospital Faculty Career Development Award and by the Brigham Research Institute and the Center for Faculty Development and Diversity's Office for Research Careers Microgrant Program.

Competing interests

D.J.M. has sponsored research from Novartis, and consults and/or has stock options/stock in J&J, Samyang Corp., Lyell, Attivare, IVIVA, and Revela; none of these relate to the topic of this manuscript. Within the past 12 months, A.M. has consulted for Janssen, PharmaEssentia, Constellation and Relay Therapeutics and receives research support from Janssen and Actuate Therapeutics. The authors confirm that there are no known conflicts of interest associated with this publication and there has been no notable financial support for this work that could have influenced its outcome. The remaining authors declare no competing interests.

Data availability

Digital data supporting the findings of this article are available at https://dataverse.harvard.edu/dataverse.xhtml?alias=Vining_et_al_2022. In vitro mouse bulk RNA-seq and human in vitro and patient-derived nanoString datasets are available at the NCBI GEO database, GEO accession code GSE206773. The following scRNA-seq datasets were utilized for analysis in this study: liver cirrhosis, GEO accession GSE136103; IPF, GEO accession GSE122960.

References

1. Distler JHW et al. Shared and distinct mechanisms of fibrosis. Nat. Rev. Rheumatol 15, 705–730 (2019). [PubMed: 31712723]
2. Leiva O et al. The role of the extracellular matrix in primary myelofibrosis. Blood Cancer J. 7, e525 (2017). [PubMed: 28157219]
3. Lampi MC & Reinhart-King CA Targeting extracellular matrix stiffness to attenuate disease: from molecular mechanisms to clinical trials. Sci. Transl. Med 10, eaao0475 (2018). [PubMed: 29298864]
4. Laklai H et al. Genotype tunes pancreatic ductal adenocarcinoma tissue tension to induce matricellular fibrosis and tumor progression. Nat. Med 10.1038/nm.4082 (2016).
5. Shin J-W & Mooney DJ Extracellular matrix stiffness causes systematic variations in proliferation and chemosensitivity in myeloid leukemias. Proc. Natl Acad. Sci. USA 113, 12126–12131 (2016). [PubMed: 27790998]
6. Vining KH & Mooney DJ Mechanical forces direct stem cell behaviour in development and regeneration. Nat. Rev. Mol. Cell Biol 18, 728–742 (2017). [PubMed: 29115301]
7. Chaudhuri O et al. Hydrogels with tunable stress relaxation regulate stem cell fate and activity. Nat. Mater 15, 326–334 (2016). [PubMed: 26618884]
8. Chaudhuri O et al. Substrate stress relaxation regulates cell spreading. Nat. Commun 6, 6364 (2015).
9. Gong Z et al. Matching material and cellular timescales maximizes cell spreading on viscoelastic substrates. Proc. Natl Acad. Sci. USA 115, E2686–E2695 (2018). [PubMed: 29507238]
10. Engler AJ, Sen S, Sweeney HL & Discher DE Matrix elasticity directs stem cell lineage specification. Cell 126, 677–689 (2006). [PubMed: 16923388]

11. Wong WJ et al. Gene expression profiling distinguishes prefibrotic from overtly fibrotic myeloproliferative neoplasms and identifies disease subsets with distinct inflammatory signatures. PLoS ONE 14, e0216810 (2019). [PubMed: 31071164]
12. Fisher DAC et al. Cytokine production in myelofibrosis exhibits differential responsiveness to JAK-STAT, MAP kinase, and NFκB signaling. Leukemia 33, 1978–1995 (2019). [PubMed: 30718771]
13. Tefferi A et al. Monocytosis is a powerful and independent predictor of inferior survival in primary myelofibrosis. Br. J. Haematol 183, 835–838 (2018). [PubMed: 29265333]
14. Jutzi JS & Mullally A Remodeling the bone marrow microenvironment—a proposal for targeting pro-inflammatory contributors in MPN. Front. Immunol 11, 2093–2093 (2020). [PubMed: 32983162]
15. Campanelli R et al. CD14brightCD16low intermediate monocytes expressing Tie2 are increased in the peripheral blood of patients with primary myelofibrosis. Exp. Hematol 42, 244–246 (2014). [PubMed: 24333662]
16. de la Guardia RD et al. Detection of inflammatory monocytes but not mesenchymal stem/stromal cells in peripheral blood of patients with myelofibrosis. Br. J. Haematol 181, 133–137 (2018). [PubMed: 28220930]
17. Brauer E et al. Collagen fibrils mechanically contribute to tissue contraction in an in vitro wound healing scenario. Adv. Sci 6, 1801780 (2019).
18. Vining KH, Stafford A & Mooney DJ Sequential modes of crosslinking tune viscoelasticity of cell-instructive hydrogels. Biomaterials 188, 187–197 (2019). [PubMed: 30366219]
19. Lee KY & Mooney DJ Alginate: properties and biomedical applications. Prog. Polym. Sci 37, 106–126 (2012). [PubMed: 22125349]
20. Rowley JA, Madlambayan G & Mooney DJ Alginate hydrogels as synthetic extracellular matrix materials. Biomaterials 20, 45–53 (1999). [PubMed: 9916770]
21. Iurlo A et al. Spleen stiffness measurement by transient elastography as a predictor of bone marrow fibrosis in primary myelofibrosis patients. Blood 124, 1825–1825 (2014).
22. Sundström G, Hultdin M, Engström-Laurent A & Dahl IMS Bone marrow hyaluronan and reticulin in patients with malignant disorders. Med. Oncol 27, 618–623 (2010). [PubMed: 19548126]
23. Jansen LE, Birch NP, Schiffman JD, Crosby AJ & Peyton SR Mechanics of intact bone marrow. J. Mech. Behav. Biomed. Mater 50, 299–307 (2015). [PubMed: 26189198]
24. Pardanani A, Begna K, Finke C, Lasho T & Tefferi A Circulating levels of MCP-1, sIL-2R, IL-15, and IL-8 predict anemia response to pomalidomide therapy in myelofibrosis. Am. J. Hematol 86, 343–345 (2011). [PubMed: 21442636]
25. Maekawa T et al. Increased SLAMF7^{high} monocytes in myelofibrosis patients harboring JAK2V617F provide a therapeutic target of elotuzumab. Blood 134, 814–825 (2019). [PubMed: 31270105]
26. Farren MR et al. Tumor-induced STAT3 signaling in myeloid cells impairs dendritic cell generation by decreasing PKCβII abundance. Sci. Signal 7, ra16–ra16 (2014). [PubMed: 24550541]
27. Garris CS et al. Successful anti-PD-1 cancer immunotherapy requires T cell–dendritic cell crosstalk involving the cytokines IFN-γ and IL-12. Immunity 49, 1148–1161.e7 (2018). [PubMed: 30552023]
28. Vasquez-Dunddel D et al. STAT3 regulates arginase-I in myeloid-derived suppressor cells from cancer patients. J. Clin. Investig 123, 1580–1589 (2013). [PubMed: 23454751]
29. Poschke I, Mougiakakos D, Hansson J, Masucci GV & Kiessling R Immature immunosuppressive CD14+HLA-DR−/low cells in melanoma patients are Stat3hi and overexpress CD80, CD83, and DC-sign. Cancer Res. 70, 4335–4345 (2010). [PubMed: 20484028]
30. Chan LLY, Cheung BKW, Li JCB & Lau ASY A role for STAT3 and cathepsin S in IL-10 down-regulation of IFN-γ-induced MHC class II molecule on primary human blood macrophages. J. Leukoc. Biol 88, 303–311 (2010). [PubMed: 20356901]
31. Humphrey JD, Dufresne ER & Schwartz MA Mechanotransduction and extracellular matrix homeostasis. Nat. Rev. Mol. Cell Biol 15, 802–812 (2014). [PubMed: 25355505]

32. Verdijk P et al. Morphological changes during dendritic cell maturation correlate with cofilin activation and translocation to the cell membrane. Eur. J. Immunol 34, 156–164 (2004). [PubMed: 14971041]
33. Kustermans G et al. Actin cytoskeleton differentially modulates NF-κB-mediated IL-8 expression in myelomonocytic cells. Biochem. Pharmacol 76, 1214–1228 (2008). [PubMed: 18789311]
34. Shutt DC, Daniels KJ, Carolan EJ, Hill AC & Soll DR Changes in the motility, morphology, and F-actin architecture of human dendritic cells in an in vitro model of dendritic cell development. Cell Motil. 46, 200–221 (2000).
35. Rullo J et al. Actin polymerization stabilizes α4β1 integrin anchors that mediate monocyte adhesion. J. Cell Biol 197, 115–129 (2012). [PubMed: 22472442]
36. Ma AD, Metjian A, Bagrodia S, Taylor S & Abrams CS Cytoskeletal reorganization by G protein-coupled receptors is dependent on phosphoinositide 3-kinase γ, a Rac guanosine exchange factor, and Rac. Mol. Cell. Biol 18, 4744–4751 (1998). [PubMed: 9671484]
37. Go Y-M et al. Phosphatidylinositol 3-kinase γ mediates shear stress-dependent activation of JNK in endothelial cells. Am. J. Physiol. Heart Circulatory Physiol 275, H1898–H1904 (1998).
38. Hannigan M et al. Neutrophils lacking phosphoinositide 3-kinase γ show loss of directionality during *N*-formyl-Met-Leu-Phe-induced chemotaxis. Proc. Natl Acad. Sci. USA 99, 3603–3608 (2002). [PubMed: 11904423]
39. Kaneda MM et al. PI3Kγ is a molecular switch that controls immune suppression. Nature 10.1038/nature19834 (2016).
40. Bartalucci N et al. Inhibitors of the PI3K/mTOR pathway prevent STAT5 phosphorylation in JAK2V617F mutated cells through PP2A/ CIP2A axis. Oncotarget 8, 96710–96724 (2017). [PubMed: 29228564]
41. Bartalucci N, Guglielmelli P & Vannucchi AM Rationale for targeting the PI3K/Akt/mTOR pathway in myeloproliferative neoplasms. Clin. Lymphoma Myeloma Leuk 13, S307–S309 (2013). [PubMed: 24290217]
42. Frausto-Del-Río D et al. Interferon gamma induces actin polymerization, Rac1 activation and down regulates phagocytosis in human monocytic cells. Cytokine 57, 158–168 (2012). [PubMed: 22137120]
43. Grove LM et al. Translocation of TRPV4-PI3Kγ complexes to the plasma membrane drives myofibroblast transdifferentiation. Sci. Signal 12, eaau1533 (2019). [PubMed: 31719171]
44. Nam S et al. Cell cycle progression in confining microenvironments is regulated by a growth-responsive TRPV4-PI3K/Akt-p27Kip1 signaling axis. Sci. Adv 5, eaaw6171 (2019). [PubMed: 31457089]
45. Rahaman SO et al. TRPV4 mediates myofibroblast differentiation and pulmonary fibrosis in mice. J. Clin. Investig 124, 5225–5238 (2014). [PubMed: 25365224]
46. Scheraga RG, Southern BD, Grove LM & Olman MA The role of TRPV4 in regulating innate immune cell function in lung inflammation. Front. Immunol 11, 1211–1211 (2020). [PubMed: 32676078]
47. Tefferi A et al. Circulating interleukin (IL)-8, IL-2R, IL-12, and IL-15 levels are independently prognostic in primary myelofibrosis: a comprehensive cytokine profiling study. J. Clin. Oncol 29, 1356–1363 (2011). [PubMed: 21300928]
48. Mullally A et al. Distinct roles for long-term hematopoietic stem cells and erythroid precursor cells in a murine model of Jak2V617F-mediated polycythemia vera. Blood 120, 166–172 (2012). [PubMed: 22627765]
49. Reyfman PA et al. Single-cell transcriptomic analysis of human lung provides insights into the pathobiology of pulmonary fibrosis. Am. J. Respiratory Crit. Care Med 199, 1517–1536 (2019).
50. Ramachandran P et al. Resolving the fibrotic niche of human liver cirrhosis at single-cell level. Nature 575, 512–518 (2019). [PubMed: 31597160]
51. Hayman AR, Macary P, Lehner PJ & Cox TM Tartrate-resistant acid phosphatase (Acp 5): identification in diverse human tissues and dendritic cells. J. Histochem. Cytochem 49, 675–683 (2001). [PubMed: 11373314]

52. Desai RM, Koshy ST, Hilderbrand SA, Mooney DJ & Joshi NS Versatile click alginate hydrogels crosslinked via tetrazine-norbornene chemistry. Biomaterials 50, 30–37 (2015). [PubMed: 25736493]
53. pheatmap: Pretty Heatmaps. R package version 1.0.12 https://github.com/raivokolde/pheatmap (2019).
54. Mullally A et al. Physiological Jak2V617F expression causes a lethal myeloproliferative neoplasm with differential effects on hematopoietic stem and progenitor cells. Cancer Cell 17, 584–596 (2010). [PubMed: 20541703]
55. Akhtar R et al. Nanoindentation of histological specimens: mapping the elastic properties of soft tissues. J. Mater. Res 24, 638–646 (2009). [PubMed: 20396607]
56. Akhtar R, Draper ER, Adams DJ & Pfaff H in Mechanics of Biological Systems and Materials Vol. 6 (eds Zavattieri P, Tekalur S & Korach C) 141–145 (Springer, 2016).
57. Cohen SR & Kalfon-Cohen E Dynamic nanoindentation by instrumented nanoindentation and force microscopy: a comparative review. Beilstein J. Nanotechnol 4, 815–833 (2013). [PubMed: 24367751]
58. Choi AP & Zheng YP Estimation of Young's modulus and Poisson's ratio of soft tissue from indentation using two different-sized indentors: finite element analysis of the finite deformation effect. Med. Biol. Eng. Comput 43, 258–264 (2005). [PubMed: 15865137]
59. Patro R, Duggal G, Love MI, Irizarry RA & Kingsford C Salmon provides fast and bias-aware quantification of transcript expression. Nat. Methods 14, 417–419 (2017). [PubMed: 28263959]
60. AnnotationDbi: manipulation of SQLite-based annotations in Bioconductor. R package version 1.46.1 https://bioconductor.riken.jp/packages/3.10/bioc/html/AnnotationDbi.html (2019).
61. RMariaDB: database interface and 'MariaDB' driver. R package version 1.0.6 https://github.com/r-dbi/RMariaDB (2018).
62. Soneson C, Love M & Robinson M Differential analyses for RNA-seq: transcript-level estimates improve gene-level inferences [version 2; peer review: 2 approved]. F1000Research 10.12688/f1000research.7563.2 (2016).
63. Love MI, Huber W & Anders S Moderated estimation of fold change and dispersion for RNA-seq data with DESeq2. Genome Biol. 15, 550 (2014). [PubMed: 25516281]
64. Luo W, Friedman MS, Shedden K, Hankenson KD & Woolf PJ GAGE: generally applicable gene set enrichment for pathway analysis. BMC Bioinf. 10, 161 (2009).
65. Swerdlow SH, International Agency for Research on Cancer & World Health Organization. WHO Classification of Tumours of Haematopoietic and Lymphoid Tissues 4th edn (International Agency for Research on Cancer, 2008).
66. Butler A, Hoffman P, Smibert P, Papalexi E & Satija R Integrating single-cell transcriptomic data across different conditions, technologies, and species. Nat. Biotechnol 36, 411–420 (2018). [PubMed: 29608179]
67. Stuart T et al. Comprehensive Integration of single-cell data. Cell 177, 1888–1902.e1821 (2019). [PubMed: 31178118]

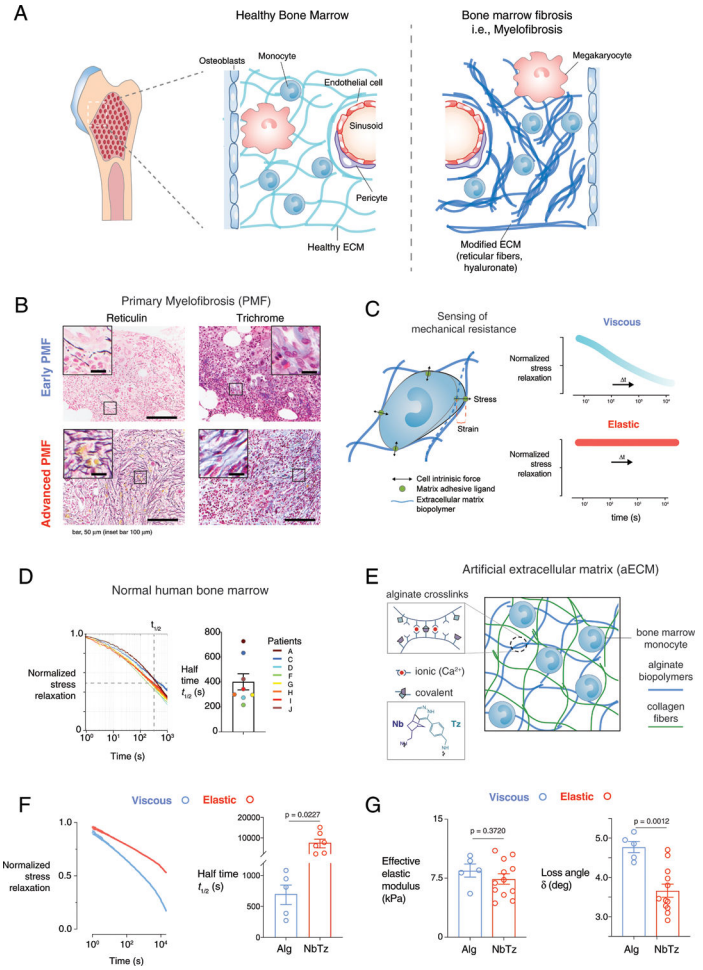

Fig. 1 |. Interpenetrating fibrillar collagen and click-modified alginate network hydrogels tune mechanical resistance of ECM.

a, In myeloproliferative neoplasms, abnormal haematopoiesis is associated with inflammation and substantial ECM remodelling (for example, myelofibrosis). **b**, Representative images of histopathology of early, prefibrotic PMF (grades 0–1) and advanced, overt (grades 2–3) PMF. PMF sections were stained for reticulin fibres (left) and trichrome stain for collagen type I (right) from a cohort of 13 patients with prefibrotic PMF and 23 patients with overt fibrosis. Scale bars, 50 μm (insets, 100 μm). **c**, Bone marrow cells sense the effective modulus (stiffness) and viscoelasticity of the matrix by its resistance to their own cell-intrinsic forces. **d**, Stress relaxation of human bone marrow (n = 8 biologically independent samples) obtained from fracture haematomas: left, normalized stress relaxation; right, half-times of stress relaxation. **e**, Artificial ECM was composed of alginate (light blue) and collagen fibres (green). Alginate was chemically modified with norbornene (Nb) and tetrazine (Tz), which covalently reinforce existing ionic (Ca^{2+}) hydrogel crosslinks to modulate viscous behaviour independently of stiffness. **f**, Normalized stress relaxation (left) and half-times of stress relaxation (right) at 10% shear strain of viscous hydrogels with only ionic crosslinking (blue) or elastic hydrogels with ionic and covalent Nb–Tz crosslinking (red). P = 0.0227 indicates statistically significant difference of unpaired t-test, Welch correction, two-tailed, n = 5 (Alg) and n = 6 (NbTz) independent

measurements. **g**, Modulus and loss angle (δ) of viscous (blue) or elastic (red) hydrogels measured by oscillatory shear rheology at 1% strain and 1 Hz. Effective elastic modulus = $2G'(1 + \nu)$, where G' is the storage modulus and $\nu = 0.5$. $P = 0.0012$ (loss angle) indicates statistical significance of unpaired *t*-test, two-tailed, $n = 5$ (Alg) and $n = 12$ (NbTz) independent measurements. Data in **d**, **f** and **g** are presented as means ± s.e.m.

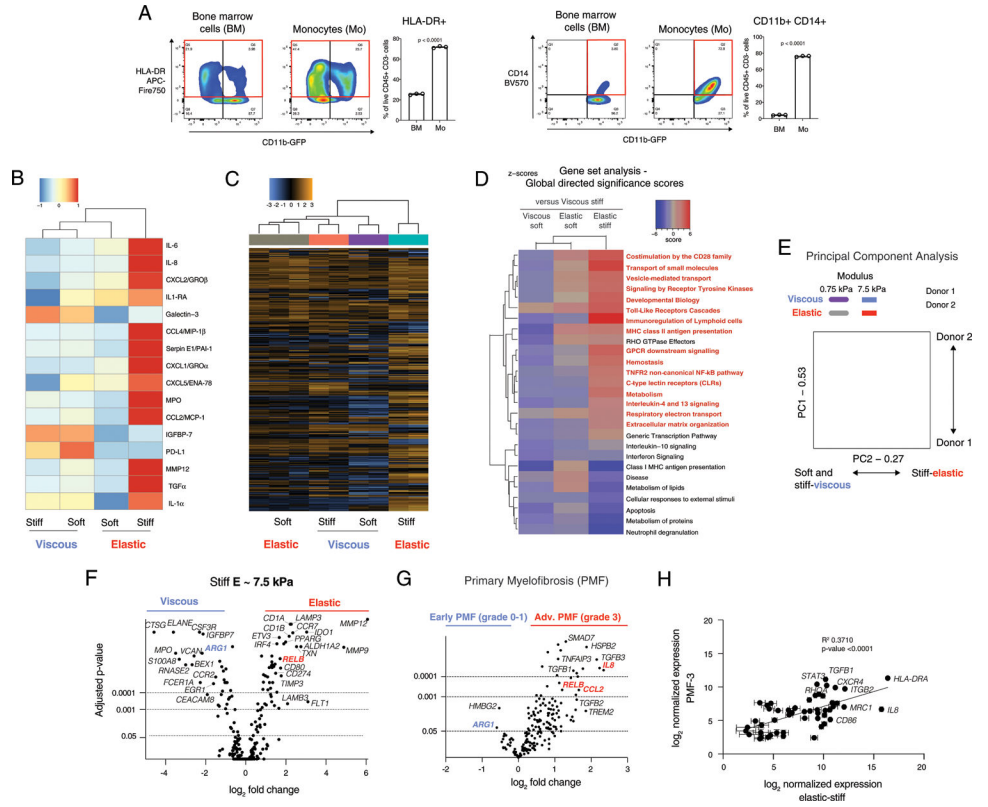

Fig. 2 |. Viscoelastic properties of ECM differentially regulate monocyte secreted cytokines and patterns of gene expression.

a, Flow cytometry of bone marrow (BM) mononuclear cells and isolated monocytes (Mo). HLA-DR versus CD11b+ is gated on live CD45+ CD3− cells (left), and CD14 versus CD11b is gated on live CD45+ CD3− CD11b+ cells (right). The red box indicates the quantified population. Statistical significance is indicated by $P < 0.0001$ with unpaired two-tailed *t*-test of $n = 3$ biological replicates from a single donor. See also Supplementary Fig. 1. **b**, Unsupervised hierarchical clustering of cytokines secreted by monocytes cultured in various matrices. Soft, ~0.75 kPa; stiff, ~7.5 kPa elastic moduli. **c**, Unbiased hierarchical clustering of gene expression of monocytes in matrices from a nanoString myeloid panel (Supplementary Data 1). **d**, Clustering of global directed significance scores of gene set analysis. **e**, Principal-component (PC) analysis of gene expression with donor 1 (closed markers) and donor 2 (open markers), $n = 2$. **f**, Volcano plots of differential gene expression comparing viscous (blue) and elastic (red) matrices of elastic modulus, $E \approx 7.5$ kPa ($n = 3$). See also Supplementary Fig. 2. **g**, Volcano plot of differential gene expression by nanoString in bone marrow from a cohort of patients with early ($n = 13$) or advanced stage, overt PMF ($n = 16$). **h**, Correlation of normalized gene expression in patients with advanced stage, overt PMF (PMF-3, $n = 16$ biologically independent samples) with monocytes in elastic, stiff matrix ($E \approx 7.5$ kPa, $n = 3$ biological replicates from a single donor). $P < 0.0001$ indicates statistically significant correlation of a linear regression. All culture analyses were performed at 3 d after encapsulation. In vitro experiments were repeated with three donors for data comparing stiff viscous and elastic gels. Two donors were tested comparing all soft and stiff, viscous and elastic gels. Data in **h** are presented as mean values ± s.e.m.

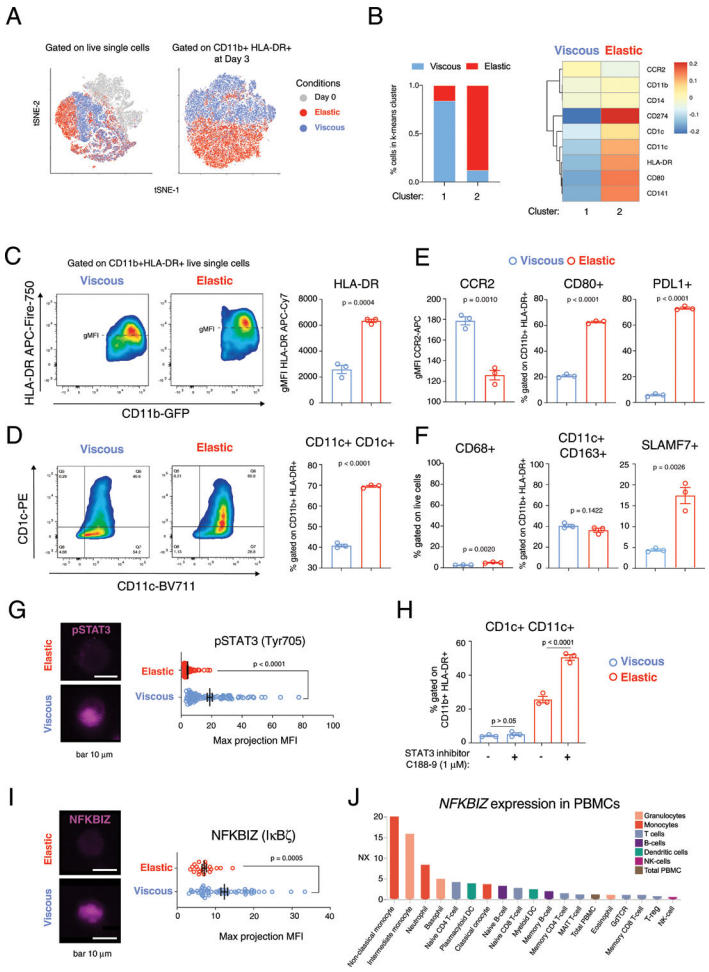

Fig. 3 |. Viscoelasticity of ECM controls dendritic cell differentiation and immature monocytes expressing pSTAT3 and an endogenous inhibitor of non-canonical NF-κB, iκBζ.

a, High-dimensional analysis of flow cytometry of cells at day 0, before encapsulation, and after 3 d in viscous or elastic gels with markers HLA-DR, CD11b, CD141, CD11c, CD1c, CD80, PDL1 and CCR2 gated on live cells (left), and gated on HLA-DR+ CD11b+ live cells (right). **b**, Relative fluorescence of cell populations in viscous and elastic gels identified by *k*-means clustering, gated on HLA-DR+ CD11b+ live cells. **c**, Flow cytometry of HLA-DR and CD11b with quantification of HLA-DR MFI on the right, gated on live cells. **d**, Dendritic cell differentiation markers, CD1c+ CD11c+, gated on CD11b+ HLA-DR+. **e**, MFI of CCR2+ and fractions of CD80+ and PDL1+ gated on CD11b+ HLA-DR+. **f**, Quantification of CD68+ cells, gated on live cells (left), and CD11c+ CD163+ (middle) and SLAMF7+ (right) cells, gated on CD11b+ HLA-DR+ cells. $n = 3$ biological replicates from a single donor for **c**–**f**, with P value from an unpaired t-test, two-tailed. **g**, Immunofluorescence imaging of pSTAT3 (Tyr705, magenta) with quantification and a $P < 0.0001$ provided by a Mann–Whitney non-parametric test, two-tailed, $n = 89$ (viscous) and $n = 95$ (elastic) biological replicates from a single donor. Scale bar, 10 µm. **h**, Flow cytometry for fraction of CD1c+ CD11c+ cells gated on CD11b+ HLA-DR+ in viscous and elastic hydrogels with and without STAT3 inhibitor C188–9 (1 µM). $n = 3$ biological replicates from a single donor, with P values from an ordinary one-way ANOVA with Tukey's

multiple comparisons. **i**, Immunofluorescence imaging of NFKBIZ (IκBζ) (magenta) with quantification and $P = 0.0005$ provided by a Mann–Whitney non-parametric test, two-tailed, $n = 57$ (viscous) and n = 22 (elastic). Scale bar, 10 μm. **j**, Gene expression of *NFKBIZ* in subsets of peripheral blood mononuclear cells (PBMCs) from the Human Blood Atlas, https://www.proteinatlas.org/humanproteome/blood. Experiments were repeated with at least three donors, unless otherwise noted. Flow staining for SLAMF7 was repeated with two donors. Data in **c**–**i** are presented as means ± s.e.m.

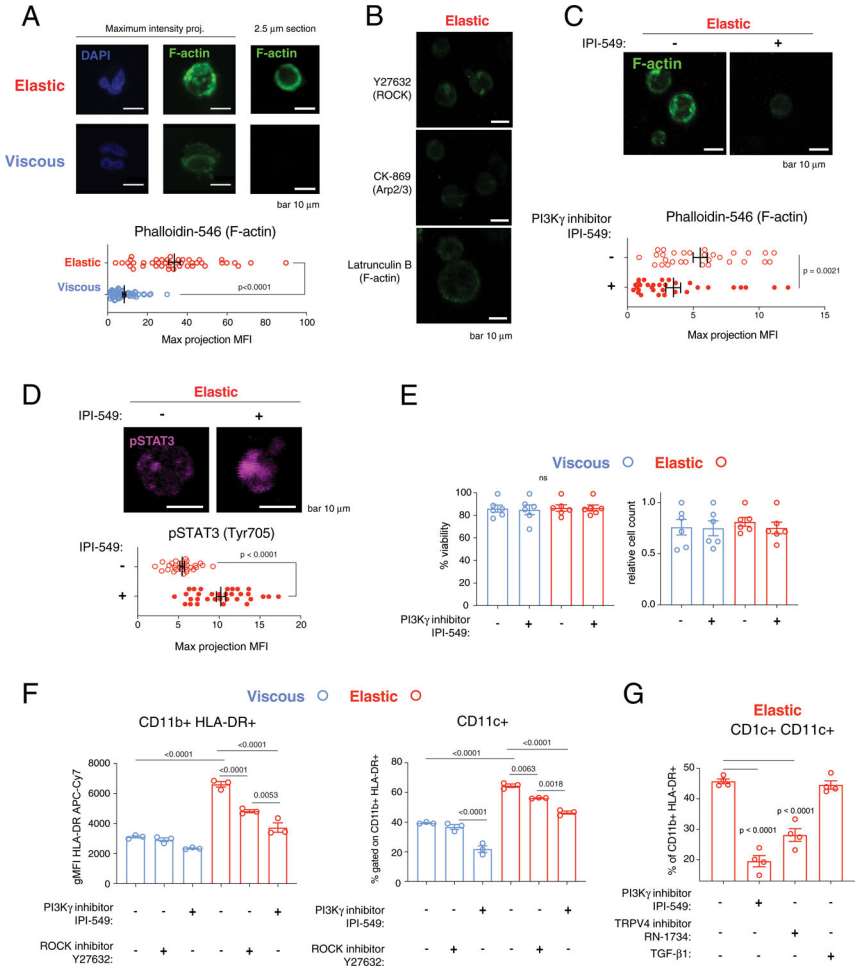

Fig. 4 |. Elasticity promotes dendritic cell differentiation through Pi3K-γ.

a, Elastic artificial ECM upregulates F-actin cortex in stiff hydrogels ($E \approx 7.5$ kPa). DAPI (blue) and F-actin staining (green, phalloidin, 1:500 stained overnight) of cells in viscous (blue) and elastic (red) hydrogels. $P < 0.0001$ indicates statistically significant difference by Mann–Whitney non-parametric test, two-tailed, $n = 57$ (viscous) and $n = 43$ (elastic) biological replicates. Scale bars, 10 μm. **b**,**c**, F-actin in elastic hydrogels with inhibition of ROCK with Y27632, Arp2/3 with CK-869, and F-actin with Latrunculin-B after 24 h in one experiment (**b**), and without and with inhibition of PI3K-γ by IPI-549 (1 μM) after 3 d (**c**). $P = 0.0021$ indicates statistically significant difference by Mann–Whitney non-parametric test, two-tailed, $n = 30$ (viscous) and $n = 32$ (elastic) biological replicates. Scale bars, 10 μm. **d**, pSTAT3 (Tyr705, magenta) in elastic hydrogels with and without IPI-549. $P < 0.0001$ indicates statistically significant difference by unpaired t-test, Welch correction, two-tailed, $n = 30$ (viscous) and $n = 32$ (elastic) biological replicates. Scale bars, 10 μm. **e**, Viability and relative cell count of cells in viscous (blue) and elastic (red) gels. $P = 0.9838$ (viability) and 0.8823 (relative cell count) from an ordinary one-way ANOVA, $n = 3$ biological replicates × 2 independent donors. NS, not significant. **f**, Flow cytometry of HLA-DR MFI and fraction of CD11b+ CD11c+ cells (gated on live-HLA-DR+) with and without IPI-549 (1 μM) or ROCK inhibitor Y27632 (10 μM). $P < 0.05$ indicate statistically significant difference

by an ordinary one-way ANOVA with Tukey's multiple comparisons, $n = 3$ biological replicates from one donor. **g**, Flow cytometry of fraction of CD11c+ CD1c+ cells (gated on live-HLA-DR-CD11b+) with IPI-549 (1 μM), RN-1734 (50 μM) or TGF-β1 (2 ng ml^{-1}). TGF-β1 is a positive control. $P < 0.05$ indicates statistically significant difference by an ordinary one-way ANOVA with Tukey's multiple comparisons, $n = 4$ biological replicates from one donor. Data in **a**, **c** and **d** were repeated with cells from three donors. Analyses in gels were performed after 3 d, unless otherwise noted. Data in **a** and **c**–**g** are presented as mean values ± s.e.m.

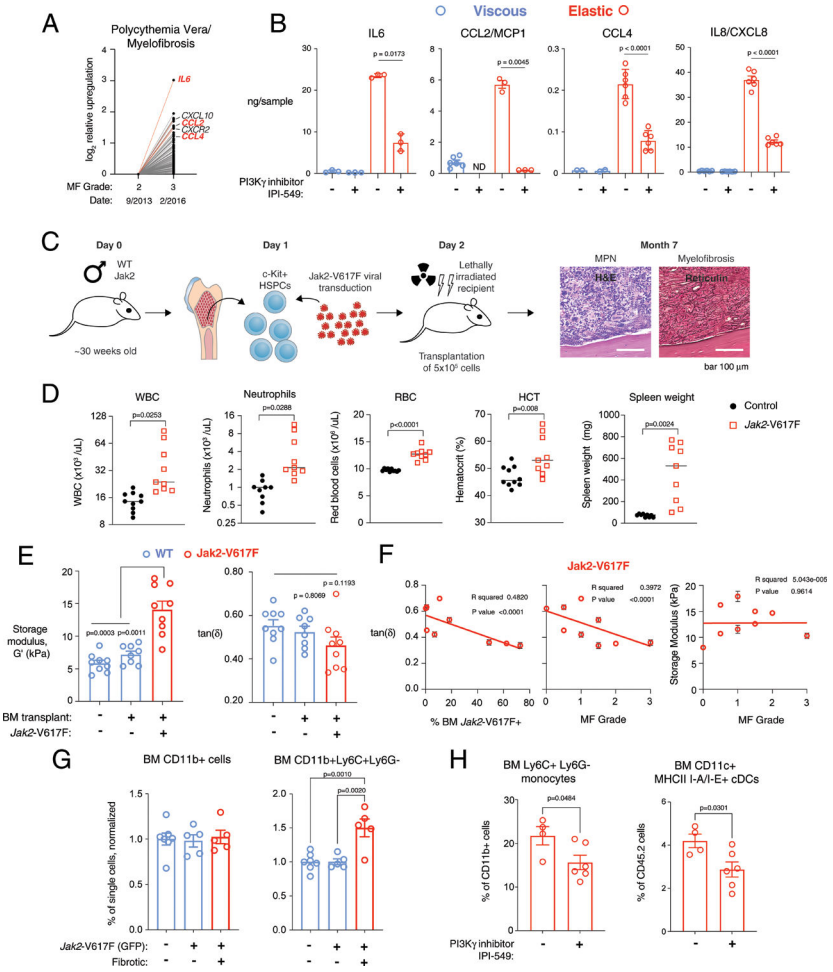

Fig. 5 |. Elasticity of ECM is associated with inflammation in MPNs and is targetable by Pi3K-γ inhibition.

a, Upregulated normalized gene expression from an untreated patient with post-polycythemia-vera myelofibrosis. **b**, Cytokines of donor monocytes in stiff, viscous and elastic hydrogels ±IPI-549. ND, not detected. *P* values indicate statistically significant difference by Brown–Forsythe and Welch ANOVA test with Dunnett's T3 multiple-comparisons test, $n = 3$ replicates from 1 donor. Repeated with three donors. **c**, Schematic of rodent transplantation model of myelofibrosis. H&E, haemotoxylin–eosin. HSPCs, haematopoietic stem and progenitor cells. Scale bars, 100 μm. **d**, Mouse peripheral blood parameters 8 weeks after transplantation with *Jak2*-V617F+ compared to wild-type cells. Spleen weight was measured 5–7 months post-transplant. $P < 0.05$ indicates statistically significant difference by unpaired *t*-test, Welch correction, two-tailed, $n = 9$ (EV) and $n = 9$ or 10 (*Jak2*-V617F). The results were consistent across three experiments. HCT, haematocrit; RBC, red blood cell; WBC, white blood cell. **e**, Nanoindentation of wild-type and transplant-recipient control (blue) or myelofibrotic (red) femur bone marrow. Mean storage modulus (left) and viscoelasticity (tan δ, right). $P < 0.05$ indicates statistically significant difference by Brown–Forsythe and Welch ANOVA with Dunnett's T3 multiple comparisons (modulus) or ordinary one-way ANOVA with Tukey's multiple comparisons (tan δ). $n = 9$ (wild-type primary mice), $n = 8$ (wild-type transplant control) and $n =$

9 (transplant retroviral *Jak2*-V617F). BM, bone marrow. **f**, Linear regression of tan δ with fraction of *Jak2*-V617F GFP+ cells in bone marrow of recipient mice (left) and myelofibrosis grading (middle), and the storage modulus (right). Data points in **e** and **f** represent mean of $n = 5$ replicates. $P < 0.05$ indicates statistically significant correlation. **g**, Normalized fraction of CD11b+ and Ly6C+ Ly6G− monocytes from empty-vector or Mx1-Cre-transplanted, non-fibrotic Mx1-Cre *Jak2*-V617F transplanted recipient controls (blue) and overtly fibrotic *Jak2*-V617F transplanted recipient bone marrow (red). Values normalized to empty-vector or Mx1-Cre transplanted controls. $P < 0.05$ indicates statistically significant difference by ordinary one-way ANOVA with Tukey's multiple comparisons, $n = 7$ (BM control), $n = 5$ (non-fibrotic *Jak2*-V617F) and n = 5 (fibrotic *Jak2*-V617F). **h**, Ly6C+ Ly6G− monocytes and CD11c+ MHC class II I-A/I-E+ conventional dendritic cells from fibrotic *Jak2*-V16F transplanted recipient bone marrow treated daily p.o. for 2 weeks with vehicle control (−) or 15 mg kg^{-1} IPI-549 (+, 10% DMSO/5% NMP/85% PEG400). $P < 0.05$ indicates statistically significant difference by an unpaired *t*-test, two-tailed, $n = 4$ (vehicle), $n = 6$ (IPI-549) from one experiment. Data in **b**, **d** and **f**–**j** are means ± s.e.m.

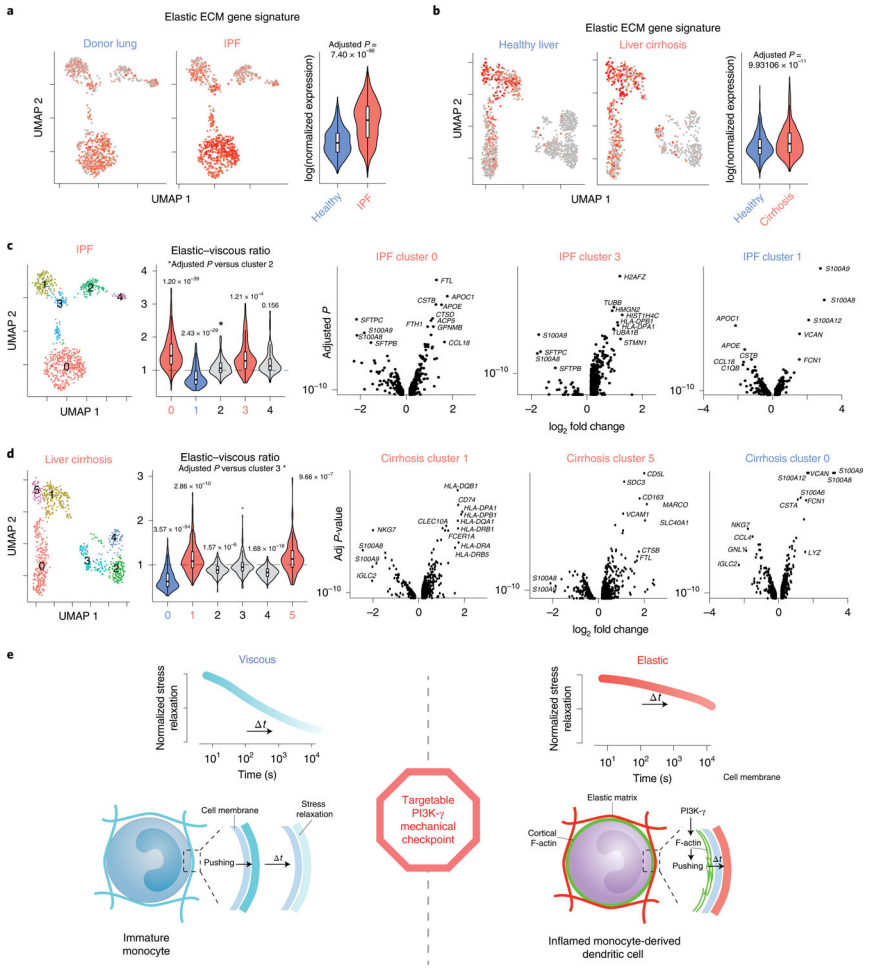

Fig. 6 |. Single-cell transcriptional profile of myeloid cells in iPF and liver cirrhosis was associated with differential gene expression regulated by viscoelasticity in vitro.

a,**b**, High-dimensional analysis of single-cell RNA-sequencing data from normal lung (n = 8) and IPF (n = 4) samples (**a**), and from normal liver (n = 5) and cirrhotic liver tissues (n = 5) (**b**). Red indicates higher expression of markers associated with cells in elastic ECM in vitro, along with their respective violin plots. FDR-adjusted $P < 0.05$ indicates statistical significance by a Wilcoxon rank sum test. NS, not significant, adjusted P value = 1. Violin plot median values: **a**, healthy = 0.0623, IPF = 0.204; **b**, healthy = −0.0190, cirrhosis = 0.00876. **c**,**d**, Unsupervised hierarchical clustering of single-cells in IPF (**c**) and liver cirrhosis (d) with violin plots showing clusters upregulated with relative elastic (red) versus viscous (blue) signatures. Volcano plots show differential gene expression of cells associated with elastic ECM (IPF, clusters 0 and 3; cirrhosis, clusters 1 and 5) or viscous ECM (IPF, cluster 1; cirrhosis, cluster 0). FDR-adjusted $P < 0.05$ indicates statistical significance by a Wilcoxon rank sum test. Violin plot median values: **c**, cluster 0 = 1.43, cluster 1 = 0.700, cluster 2 = 0.981, cluster 3 = 1.91, cluster 4 = 1.06; **d**, cluster 0 = 0.611, cluster 1 = 1.07, cluster 2 = 0.887, cluster 3 = 0.960, cluster 4 = 0.825, cluster 5 = 1.12. **e**, Proposed mechanical checkpoint of monocyte cell fate transduces external mechanical resistance to promote dendritic cell differentiation. Monocytes engage with the surrounding ECM by cell-intrinsic pushing forces. F-actin reorganization in response to

extracellular viscoelasticity is driven by PI3K-γ signalling. In viscous ECM, cell-generated stresses rapidly relax, and cells resemble immature monocytes in native bone marrow. With increased ECM elasticity, cellular stresses relax much more slowly, which leads to enhanced proinflammatory polarization and differentiation towards dendritic cells.